

Active Inference Tree Search in Large POMDPs

Domenico Maisto¹, Francesco Gregoretti², Karl Friston³, Giovanni Pezzulo^{1,*}

1) Institute of Cognitive Sciences and Technologies, National Research Council, Via San Martino della Battaglia 44, Rome 00185, Italy

2) Institute for High Performance Computing and Networking, National Research Council, Via Pietro Castellino 111, Naples 80131, Italy

3) The Wellcome Centre for Human Neuroimaging, Institute of Neurology, University College London, London, WC1N 3AR UK

* Corresponding author:

Giovanni Pezzulo

ISTC-CNR

Via San Martino della Battaglia 44, 00185 Rome, Italy

Email: giovanni.pezzulo@istc.cnr.it

Phone: +39 6 44595206

Abstract

The ability to plan ahead efficiently is key for both living organisms and artificial systems. Model-based planning and prospection are widely studied in cognitive neuroscience and artificial intelligence (AI), but from different perspectives—and with different desiderata in mind (biological realism versus scalability) that are difficult to reconcile. Here, we introduce a novel method to plan in POMDPs—*Active Inference Tree Search* (AcT)—that combines the normative character and biological realism of a leading planning theory in neuroscience (Active Inference) and the scalability of tree search methods in AI. This unification enhances both approaches. On the one hand, tree searches enable the biologically grounded, first principle method of active inference to be applied to large-scale problems. On the other hand, active inference provides a principled solution to the exploration–exploitation dilemma, which is often addressed heuristically in tree search methods. Our simulations show that AcT successfully navigates binary trees that are challenging for sampling-based methods, problems that require adaptive exploration, and the large POMDP problem ‘*RockSample*’—in which AcT reproduces state-of-the-art POMDP solutions. Furthermore, we illustrate how AcT can be used to simulate neurophysiological responses (e.g., in the hippocampus and prefrontal cortex) of humans and other animals that solve large planning problems. These numerical analyses show that *Active Tree Search* is a principled realisation of neuroscientific and AI planning theories, which offer both biological realism and scalability.

Keywords: Active Inference, Tree Search, model-based planning, POMDP

1 Introduction

Model-based planning problems have received substantial attention in various disciplines, including AI, machine learning, robotics, cognitive science and neuroscience. The interdisciplinary exchanges between these disciplines have been numerous (Daw & Dayan, 2014; Geffner, 2013, 2018; Pezzulo et al., 2019; Russell & Norvig, 2002; Sutton & Barto, 1998), but yet we still lack a theoretical synthesis that unites their desiderata (e.g., biological realism in neuroscience versus efficiency in AI) (Hassabis et al., 2017). Here, we take a step in this direction by showing that a prevalent theory of model-based control and planning in neuroscience—active inference (Parr et al., 2022)—can be extended straightforwardly to address large-scale planning problems using tree search methods. Our novel approach—*Active Inference Tree Search* (AcT)—bridges computational neuroscience and AI requirements by combining the normative character and biological realism of active inference with the scalability and efficiency of tree search methods.

Active inference is an increasingly popular computational neuroscience framework that characterises perception, action, and planning in terms of approximate (variational) Bayesian inference under a generative model (K. Friston et al., 2015, 2017, 2020; K. J. Friston, 2010). Active inference is related to a family of recent approaches to solving POMDP problems in machine learning and AI, which exploit a general duality between control and inference problems (Todorov, 2008) and which include *control as inference* (Levine, 2018; Rawlik et al., 2013), *planning as inference* (Attias, 2003a; Botvinick & Toussaint, 2012), *risk-sensitive* and *KL control* (Kappen et al., 2012). A peculiarity of active inference is that it implements a principled form of model-based planning: it infers posteriors over action sequences (or policies) by considering an *expected free energy* functional, which effectively balances exploration and exploitation in a context-sensitive and optimal fashion. Previous studies have established that the computations underlying active inference are biologically plausible and can reproduce various findings in functional brain anatomy, neuronal dynamics and behaviour (K. Friston et al., 2017; K. J. Friston et al., 2014; K. J. Friston, Parr, et al., 2017; Pezzulo et al., 2018), as well as furnishing sophisticated forms of inference under hierarchical and temporally deep generative models (Clark, 2015; K. Friston et al., 2020; K. J. Friston, Parr, et al., 2017; K. J. Friston, Rosch, et al., 2017; Millidge, 2019a; Pezzulo et al., 2018; Ueltzhöffer, 2017).

However, the active inference framework has been developed with cognitive and biological realism in mind, not scalability or implementational efficiency. Its current implementations require the exhaustive evaluation of all allowable policies and hence can only address small-scale POMDP problems. Here, we develop an extension of active inference aiming to address larger POMDPs: *Active Inference Tree Search* (AcT). Our novel algorithm retains the key aspects of active inference—namely, the use of expected free energy to infer the posterior probability of policies—but relaxes the exhaustive evaluation of all policies, using tree search planning methods that are popular in AI (Daw & Dayan, 2014; Geffner, 2013, 2018; Pezzulo et al., 2019; Russell & Norvig, 2002; Sutton & Barto, 1998).

Tree search AI methods perform a look-ahead search over a planning tree, which describes the possible courses of actions and their associated outcome values. The tree is expanded during planning from the root node (i.e., the state where planning starts) to the leaves. In most practical applications, the tree cannot be explored exhaustively. Various heuristic procedures have been proposed to decide

what actions to consider next, how to expand the planning tree, and how to balance exploration and exploitation to find an almost-optimal sequential policy (Kearns et al., 2002; Kocsis & Szepesvári, 2006). A common way to approximate the value of possible policies is using Monte-Carlo sampling (Gelly & Silver, 2011), which permits sampling rewards obtained by following a given branch of the tree (corresponding to a given course of action) and storing their statistics in the tree nodes. We will show that *Active Inference Tree Search* can contextualise these heuristic methods within a normative and biologically realistic approach, using an (expected) free energy functional that automatically entails the appropriate level of exploration, rendering the use of Monte Carlo methods unnecessary.

The main contribution of this article is a proof of principle that the novel AcT method—that combines active inference and tree search—can augment both approaches. On the one hand, using a planning tree enables active inference to handle larger problems than previously. On the other hand, active inference provides a principled approach to dissolve the exploration-exploitation dilemma, which is addressed heuristically in tree search methods.

In the following Sections, we first review tree search planning methods in AI and active inference. We then introduce *Active Inference Tree Search* formally and validate it using three simulations, showing that it can handle (i) deceptive binary trees (that are challenging for sampling-based methods), (ii) problems that require adaptive exploration, and (iii) larger-scale POMDP problems (i.e., *RockSample*). Finally, to highlight the potential of *Active Inference Tree Search* for studying biological phenomena, we use the scheme to simulate neuronal responses in humans (and other animals) that solve large planning problems.

2. Methods: technical background

2.1 Partially observed Markov decision processes (POMDP)

Several real world and biological problems can be cast as sequential decisions under uncertainty. Formally, they can be treated as extensions of Markov Decision Process, where the observed action outcomes provide only partial information about the state of the environment; this corresponds to the framework of Partially Observed Markov Decision Process (POMDP) (Sutton & Barto, 1998).

A POMDP can be defined as a tuple $\langle S, A, T, Z, O, R \rangle$ where:

- S denotes the set of environment states that generate information for the agent to accomplish a task;
- A is the set of actions potentially executable by the agent;
- $T : S \times A \times S \rightarrow [0,1]$, such that $T(s, a, s') = \text{Pr}(s'|s, a)$, is the transition probability of being in a state s' after performing the action a from state s ;
- Z denotes the set of observations.

- $O : S \times A \times Z \rightarrow [0, 1]$, such that $O(s', a, z) = Pr(z|a, s')$, is the probability of observing $z \in Z$ by performing an action a in state s' ;
- $R : S \times A \rightarrow \mathbb{R}$, where $R(s, a)$ is the reward obtained by taking the action a from a particular state s (Sutton & Barto, 1998).

In a POMDP, the state of the environment cannot be observed directly but can be inferred based on partial observations that the agent solicits through action. Since the agent's state information can be noisy or incomplete, it is helpful for an agent to consider a probability distribution over the states it could be in. This probability distribution, called a (Bayesian) *belief*, is defined as the posterior $b_t(s) = Pr(s_t = s|h_t, b_0)$ given the initial belief b_0 and a complete sequence or *history* $h_t = \{a_0, z_1, \dots, z_{t-1}, a_{t-1}, z_t\}$ of past actions and observations. At any time t , it is possible to write down the belief state b_t as a Bayesian update $\tau(b_{t-1}, a_{t-1}, z_t)$ of the previous belief state b_{t-1} , given the action a_{t-1} and the current observation z_t .

Generally, solving a POMDP problem means finding a *plan* or *policy* by predicting the situations the agent could encounter in the future, conditioned on the actions it executes. One can specify a policy as a function $\pi : \mathcal{B} \rightarrow A$ that associates beliefs $b \in \mathcal{B}$ to actions $a \in A$. In Reinforcement Learning (RL), the value function $V_\pi(b)$ of a policy π , evaluated starting from an initial belief b , corresponds to the expected total discounted reward $V_\pi(b) = \mathbb{E}[\sum_{t=0}^T \delta^t R(s_t, \pi(b_t))]$, where $\delta \in (0, 1]$ is a discount factor, and T is a finite (or infinite) value if the POMDP problem has a finite (or infinite) time horizon. Following the RL setup, a POMDP plan or policy is optimal when π^* maximises the value function $V_{\pi^*}(b)$.

2.2 Online POMDP planning

There are two main approaches to POMDP problems: offline and online. In offline methods (Pineau et al., 2003)(Spaan & Vlassis, 2005)(Shani et al., 2013)(Brock et al., 2009), the policy is computed before execution by considering every possible belief state. Offline methods achieve good results for small-size scenarios but are not suitable for large POMDP problems. In online methods, there is an alternation between policy construction, whose goal is discovering a good short-path policy (often a single action) for the current belief; and execution, where the selected policy is executed. These methods scale up to large POMDP problems but usually result suboptimal policies, as they are computed based on a subset of beliefs. The two approaches are complementary and can coexist. For example, online methods can be complemented by initial approximations acquired via some offline algorithm. However, online methods are generally more widely used, given their scalability.

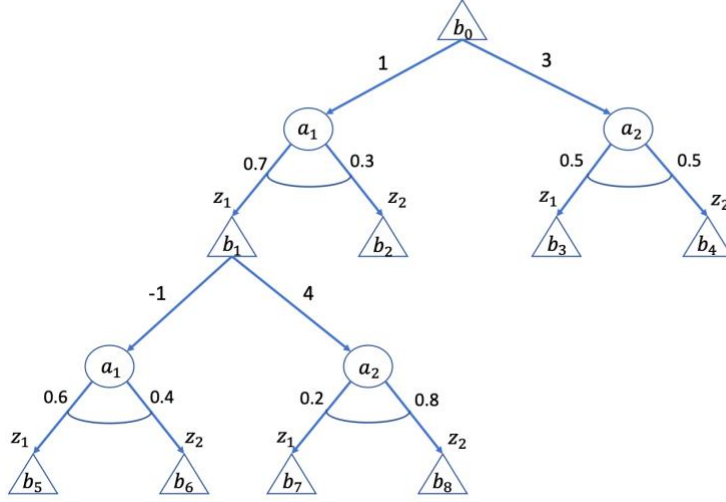


Figure 1. AND-OR tree for a POMDP with 2 observations $\{z_1, z_2\}$ and 2 actions $\{a_1, a_2\}$. Triangular (OR) nodes represent belief states, whereas circular (AND) nodes represent actions. The numerical values shown on the edges that stem from OR-nodes represent rewards $R(b, a)$, whereas the numerical values shown on the edges that stem from AND-nodes represent conditional probabilities $P(z|b, a)$.

Ross et al. (Ross, Pineau, Paquet, et al., 2008) established a general scheme for online planning algorithms. In their scheme, every online algorithm can be understood as a procedure in which policy construction is a routine implementing a predefined set of steps: 1) visit, 2) expansion and 3) estimation of an AND-OR tree, with the OR nodes representing beliefs and nodes corresponding to actions (Figure 1). The algorithm starts by setting the current belief as the *root* node of a tree; then builds new belief nodes generated by action nodes. Every time a new belief node is allocated, it is evaluated, and its value is transmitted up to the belief ancestors—up to the root—to update the value of the corresponding policy (i.e., action sequence corresponding to a specific branch of the tree).

The most popular online-planning approaches are Heuristic Search, Branch-and-Bound pruning, and Monte Carlo sampling (Ross, Pineau, Paquet, et al., 2008). In Heuristic Search methods (Smith & Simmons, 2004)(Ross, Pineau, & Chaib-draa, 2008), a routine explores the belief tree using a heuristic to detect relevant nodes to branch out (frequently, for a single forward step). It successively updates the heuristic value associated with its ancestors (which differs between heuristic search algorithms). However, this procedure can be computationally expensive, reducing the effectiveness of the heuristic-based node selection. Branch-and-bound approaches instead rely on a general search technique that constrains the search tree expansion by pruning suboptimal branches (Paquet et al., 2005). They assign every belief tree node an upper and a lower bound of a quality value function. If a branch leads to a node with an upper bound—that is lower than the lower bound of another node of a different branch—then the first node is labelled as the root of a suboptimal subtree that can be pruned. Finally, Monte Carlo algorithms randomly sample a subset of observations each time. This procedure constrains the branching expansion of the belief tree and the depth of the search.

While Monte Carlo algorithms follow the same general procedure, they sample outcomes in different ways (McAllester & Singh, n.d.)(Yoon et al., 2008). One of the earliest Monte-Carlo-sampling-based

algorithms for solving POMDP—the Sparse Sampling algorithm of Kearns et al. (Kearns et al., 2002)—builds a fixed depth tree search in one stage (i.e., from the root to the leaves) using a "black-box" simulator (a generative model) for modelling state transitions and simulating reward returns. To improve the performance of the Sparse Sampling algorithm, Kocsis and Szepesvári proposed the Upper Confidence Tree (UCT) algorithm (Kocsis & Szepesvári, 2006), which introduced two essential novelties. First, it uses Monte Carlo Tree Search (MCTS) (Browne et al., 2012): a rollout-based Monte Carlo planning method inspired by game strategy searches but builds the belief tree progressively and iteratively. Second, it selects actions during the planning phase in a stochastic way rather than by drawing from a uniform distribution (which is consistent with theoretical results on sequential decision making under uncertainty (Auer et al., 2002)).

2.3 Related works

UCT (Browne et al., 2012) is an online decision-making algorithm that works by constructing a tree of simulated histories h_t that expands from an initial belief state b_0 cast as root, and alternating state and action nodes, eventually drawn by a *generative model*, i.e., a probabilistic model that statistically describes the POMDP distributions T and Z . To select which node (and branch corresponding to some history h_t) to expand next in $h_t a = \{a_0, z_1, \dots, z_t, a_{t+1}\}$, the algorithm uses the value function $V_\pi(h_t a)$ and evaluates the expected return from the initial belief b_0 following the policy π furnished by h . A peculiarity of UCT, as of every MCTS algorithm, is the way the value function $V_\pi(h_t a)$ is calculated. Instead of bootstrapping $V_\pi(h_t a)$ using dynamic programming, it is estimated by Monte Carlo sampling, where multiple stochastic rollouts approximate a mean value. The computed value is then propagated back to each branch node and averaged with contributions from other histories branching off from the same node. Concurrently, a visitation count $N(h_t a)$ is updated, such that $N(h_t) = \sum_a N(h_t a)$ is the number of simulations ran through the node representing s . In UCT, node visit counts are used effectively: node selection is seen as a Multi-armed Bandit problem for which the optimal choice uses the Upper Confidence Bound (UCB) $V_\pi(h_t a) + c_p \sqrt{\log N(h_t) / N(h_t a)}$. UCB augments the value function with an exploration term favouring less-visited nodes (Auer et al., 2002).

A UCT-based planning algorithm that has received attention in the last decade is POMCP (Silver & Veness, 2010). POMCP can handle POMDPs with large state spaces. It adopts MCTS to generate an AND-OR belief tree, where the AND nodes (actions) are selected through the UCB algorithm, and the OR nodes represent a set of sampled states (not a full probability distribution), which are iteratively maintained by a particle filter. Although it can handle problems of considerable size, POMCP has some implicit limitations. By representing the POMDP problem as a belief tree, POMCP needs to visit every potential observation related to a belief state at least once. Furthermore, as it uses the UCB heuristic, its worst-case is computationally challenging (Coquelin & Munos, 2014).

DESPOT (Ye et al., 2017) is another state-of-art MCTS-based algorithm that tries to overcome (at least theoretically) the above limitations by operating on a sparse belief tree generated on a subset of sampled observations. As in POMCP, the nodes of such a reduced tree—called DESPOT tree—approximate distributions over belief states using particles. An MCTS planning routine progressively constructs the DESPOT tree by iterating the following three stages: a forward search that traverses

the tree until it encounters a leaf node according to the heuristic values (which includes a pre-computed regularisation term to prevent overfitting); a leaf initialisation, where a Monte Carlo sampling estimates the upper and lower bounds of the selected leaf node; and a backup, that passes back through the path tracked in the forward search and updates the upper and lower bounds of each visited node, according to the Bellman optimality principle. These three stages are analogous to the selection, expansion, and backpropagation phases of POMCP. However, they are iterated until the difference between the upper and lower bounds of the belief root state is sufficiently small (as in a Branch-and-Bound method).

More recently, new approaches to online POMDP planning allow the parallelisation of extant methods (Cai et al., 2018)(Lee & Kim, 2016) or use deep learning to extract and aggregate relevant information from the environment to speed up and improve policy inference (Igl et al., 2018)(Karkus et al., 2017). Furthermore, applied research in decision making for autonomous urban vehicles has engendered novel solutions to the online POMDP and approximate solutions (Galceran et al., 2017)(Schwartz et al., 2018)(Badue et al., 2019).

2.4 Active inference

Active inference is a formal framework that integrates the cybernetic concepts of feedback and error control (Wiener, 1948) with a Bayesian inferential scheme (Pezzulo et al., 2015, 2018; Seth, 2014). In active inference, perception and action (or policy) selection form a closed-loop process. Its execution can be cast in terms of approximate Bayesian inference (Botvinick & Toussaint, 2012; Donnarumma et al., 2016; Pezzulo, Donnarumma, et al., 2017; Pezzulo et al., 2013), which is rendered tractable using a variational approximation under the free-energy-minimisation principle; i.e., a variational principle of least action (K. Friston et al., 2012). The active inference scheme has been proposed in many variants, and its biological plausibility is under investigation (K. Friston et al., 2017)(K. J. Friston, FitzGerald, Rigoli, Schwartenbeck, O’Doherty, et al., 2016).

In its essence, active inference is a theory of decision-making under uncertainty (i.e., “[...] a formal treatment of choice behaviour based on the premise that agents minimise the expected free energy of future outcomes.” (K. Friston et al., 2015)). As discussed in (K. Friston et al., 2012), it can be cast in terms of optimal decision theory and described as a POMDP where the agent holds beliefs about the probability of associating observations to hidden states, and where rewards or cost functions are absorbed into beliefs about initial state distribution and terminal observations.

In this setting, active inference can be formally represented by a tuple $\langle S, O, U, \gamma, R, P, Q \rangle$ where:

- S is the set of agent’s hidden states s by which the agent infers the environmental state. Where a sequence of hidden states is denoted by $\tilde{s} = (s_0, \dots, s_T)$;
- O is a finite set of observations (or outcomes) o , and $\tilde{o} = (o_0, \dots, o_T)$;

- U is a finite set of *control states* u executable by the agent to control the environment. A sequence of *control states* $\tilde{u} = [u_t, \dots, u_T]$ is called *policy* and denoted as π . Thus, $\pi = \tilde{u} = [\pi^{(t)}, \dots, \pi^{(T)}]$;
- $\gamma \in \mathbb{R}$, is an additional variable denoted as *precision*, introduced to self-tune the control-state selection process adaptively;
- $R(\tilde{o}, \tilde{s}, \tilde{u})$ is a *generative process* that generates probabilistic outcomes from hidden states and actions;
- $P(\tilde{o}, \tilde{s}, \tilde{u}, \gamma | \Theta)$ is a *generative model* with parameters $\Theta = \{\mathbf{A}, \mathbf{B}, \mathbf{C}, \mathbf{D}, \alpha, \beta\}$ (defined later on), over outcomes, hidden states, control states and precision;
- $Q(\tilde{s}, \tilde{u}, \gamma)$ is an approximate posterior distribution over states, control states and precision, with expectations $(\mathbf{s}_0^\pi, \dots, \mathbf{s}_T^\pi, \boldsymbol{\pi}, \boldsymbol{\gamma})$.

It is worth noting that there is a fundamental difference between the *generative process* and *generative model*. The *generative process* describes transitions between states of the environment as a function of the agent's actions and generates observed outcomes. The *generative model* describes the agent's beliefs about the world and encodes states and policies as expectations. In other words, in active inference, an agent adopts an internal *generative model* to understand its observations and how they may be generated by external environmental dynamics (*generative process*).

A second important difference is between *control states* (or policies), which are part of the generative model, and *actions*, which are part of the generative process. This formulation permits casting action in terms of beliefs about policies and converting an optimal control problem into an optimal inference problem, a.k.a. planning as inference (Attias, 2003b).

2.4.1 Generative models for active inference

As shown in Fig. 2, the generative model used in active inference includes hidden *states* s as causes of the observed outcomes o . Hidden states move forward in time under a policy π that depends on the precision γ . A series of factorisations permits writing down the model's joint density as:

$$P(\tilde{o}, \tilde{s}, \tilde{u}, \gamma | \Theta) = P(\gamma | \Theta) P(\pi | \gamma, \Theta) \prod_{t=0}^T P(o_t | s_t, \Theta) P(s_t | s_{t-1}, \pi, \Theta) \quad (1)$$

where:

$$P(o_t | s_t, \Theta) = \mathbf{A}$$

$$P(s_{t+1} | s_t, \pi, \Theta) = \mathbf{B}(u_t = \pi^{(t)}) \text{ for } t > 0 \text{ and } P(s_0 | \Theta) = \mathbf{D} \text{ otherwise} \quad (2)$$

$$P(\pi|\gamma, \Theta) = \sigma(\ln \mathbf{E} - \gamma \cdot \mathbf{G}_\pi|\Theta)$$

$$P(\gamma|\Theta) \sim \Gamma(\alpha, \beta)$$

In Equations (2), the matrix \mathbf{A} encodes the likelihood of observations given a hidden state, while \mathbf{C} represents their prior distribution. State transitions are specified by \mathbf{B} , the prior distribution of the initial state is given by \mathbf{D} , and \mathbf{E} is the prior expectation of each policy. Finally, α and β correspond to the shape and the rate parameters of the gamma density, which underlies the γ -distribution, respectively.

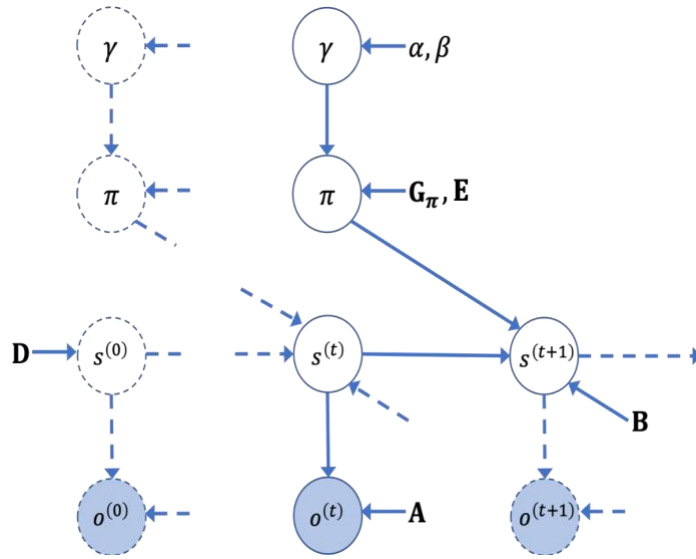


Figure 2. Graphical model for active inference. See the main text for an explanation.

The quantity \mathbf{G}_π is a score of the “quality” of a generic policy. It can be viewed as the log prior of a given policy, conditioned on the future state and observations, together with preferred outcomes (see below for more details).

2.4.2 Approximate posterior and variational inference

Active inference uses a variational approximation for Bayesian inference (Beal, 2003). This implies two key things. First, active inference uses an *approximate posterior* over hidden states and parameters $(\tilde{s}, \tilde{u}, \gamma)$, which can be described in factorised form (known as a mean field approximation):

$$Q(\tilde{s}, \tilde{u}, \gamma) = Q(\pi)Q(\gamma) \prod_{t=0}^T Q(s_t|\pi); \quad (3)$$

where the sufficient statistics are encoded by the expectations $\boldsymbol{\mu} = (\tilde{s}^\pi, \pi, \gamma)$, with $\tilde{s}^\pi = s_0^\pi, \dots, s_T^\pi$. Second, active inference performs a minimisation of *variational free energy* of the generative model

with respect to the sufficient statistics $\boldsymbol{\mu}$ of its approximate posterior $Q(\tilde{s}, \tilde{u}, \gamma)$. By exploiting some mathematical identities, the variational free energy function can be defined as follows, where

$$\begin{aligned} F(\tilde{o}, \tilde{s}^\pi, \boldsymbol{\pi}, \boldsymbol{\gamma}) &= \mathbb{E}_Q[\ln Q(\tilde{s}^\pi, \boldsymbol{\pi}, \boldsymbol{\gamma}) - \ln P(\tilde{o}, \tilde{s}^\pi, \boldsymbol{\pi}, \boldsymbol{\gamma}|\Theta)] \\ &= D_{\text{KL}}[Q(\tilde{s}^\pi, \boldsymbol{\pi}, \boldsymbol{\gamma})||P(\tilde{s}^\pi, \boldsymbol{\pi}, \boldsymbol{\gamma}|\tilde{o}, \Theta)] - \ln P(\tilde{o}|\Theta) \\ &\geq -\ln P(\tilde{o}|\Theta) \end{aligned} \quad (4)$$

$\mathbb{E}_Q[\cdot]$ denotes an expected value under Q , $D_{\text{KL}}[\cdot||\cdot]$ is the Kullback-Leibler divergence, and $-\ln P(\tilde{o}|\Theta)$ (i.e., the negative logarithm of the *model evidence* $P(\tilde{o}|\Theta)$) is called self-information, surprisal or, more simply, *surprise*. When $Q(\tilde{s}^\pi, \boldsymbol{\pi}, \boldsymbol{\gamma})$ converges on the posterior $P(\tilde{s}^\pi, \boldsymbol{\pi}, \boldsymbol{\gamma}|\tilde{o}, \Theta)$, the variational free energy decreases. If they match exactly, and their divergence is zero, free energy becomes surprise. Therefore, one could summarize the variational inference as minimizing free energy to approximate the posterior while, at the same time, evaluating a bound on log-model evidence (often called *evidence bound* in machine learning).

Note that the variational approach transforms inference (namely, calculating posterior from prior beliefs) into an optimization problem (namely, finding sufficient statistics $\boldsymbol{\mu}$ such that the corresponding free energy is minimum). It is possible to demonstrate (Parr et al., 2022) that such a condition is satisfied when the sufficient statistics at any time t are:

$$\begin{aligned} \mathbf{s}_t^\pi &\approx \sigma(\ln \mathbf{A} \cdot \mathbf{o}_t + \ln(\mathbf{B}(\pi^{(t-1)}) \cdot \mathbf{s}_{t-1}^\pi)) \\ \boldsymbol{\pi} &= \sigma(\ln \mathbf{E} - \boldsymbol{\gamma} \cdot \mathbf{G}_\pi) \end{aligned} \quad (5)$$

$$\boldsymbol{\gamma} = \frac{\alpha}{\beta - \mathbf{G}_\pi}$$

Here, we use the symbol “ \cdot ” to denote the inner product, defined as $\mathbf{A} \cdot \mathbf{B} = \mathbf{A}^T \mathbf{B}$, where \mathbf{A} and \mathbf{B} are two arbitrary matrices. The first equation defines the expected hidden state and corresponds to the part of active inference that implements perception. The second equation derives (as the expected hidden state) from a Boltzmann distribution of the policies' quality values. The expected value of γ is the distribution's sensitivity (or inverse temperature parameter): it adjusts the tendency to select a policy with greater or lesser confidence. The last equation tunes the expected precision value on the base of policy quality values (in a nonbiological setting, this precision is usually set to 1, especially for policies that only look ahead).

The term \mathbf{G}_π is the policies' *expected free energy* (EFE). It is used to score the quality of a generic policy with respect to the future outcomes and states that are expected under such policies. The EFE \mathbf{G}_π occurs in each of the three above equations. In the first equation, it controls the optimism bias. In the second equation, EFE determines the choice of policies. Finally, in the third equation, EFE nuances an agent's confidence about action selection. With greater differences among the values of \mathbf{G}_π , the precision is greater—and the agent is more confident about what to do next (in a non-biological setting, the selected policy is the one with the smallest EFE).

Note a fundamental difference between active inference and RL based approaches to POMDP: RL approaches are based upon a value *function* of future states, while active inference infers the best policy using an expected free energy *functional of beliefs* about future states. Technically, this means replacing the Bellman optimality principle with a straightforward principle of least action, where the action is the path integral of expected free energy. Teleologically, this means active inference considers optimal sequences of belief states that subsume information-seeking and preference-seeking imperatives into the same functional, thereby dissolving the exploration–exploitation dilemma.

One can evaluate \mathbf{G}_π by integrating the expected free energy—under the policy π —from the current instant t to some horizon T :

$$\mathbf{G}_\pi = \sum_{\tau=t}^T G(\pi, \tau) \quad (6)$$

where

$$\begin{aligned} G(\pi, \tau) &= F_\tau(\pi) \\ &= \mathbb{E}_{\tilde{Q}}[\ln Q(s_\tau|\pi) - \ln P(o_\tau, s_\tau|\pi, C)] \\ &= \mathbb{E}_{\tilde{Q}}[\ln \ln Q(s_\tau|\pi) - \ln P(s_\tau|o_\tau, \pi) - \ln P(o_\tau|C)] \\ &\geq \mathbb{E}_{\tilde{Q}}[\ln Q(s_\tau|\pi) - \ln Q(s_\tau|o_\tau, \pi)] - \mathbb{E}_{\tilde{Q}}[\ln P(o_\tau|C)] \\ &= \mathbb{E}_{\tilde{Q}}[\ln Q(o_\tau|\pi) - \ln Q(o_\tau|s_\tau, \pi)] - \mathbb{E}_{\tilde{Q}}[\ln P(o_\tau|C)] \\ &= -D_{\text{KL}}[Q(o_\tau|\pi)||P(o_\tau)] - \mathbb{E}_{\tilde{Q}}[H[P(o_\tau|s_\tau)]] \end{aligned} \quad (7)$$

Here, $\mathbb{E}_{\tilde{Q}}[\cdot]$ is the expected value under the predicted posterior distribution $\tilde{Q} = Q(o_\tau, s_\tau | \pi) \triangleq P(o_\tau | s_\tau)Q(s_\tau | \pi)$ over hidden states and their outcomes under a specific policy π . The final identity in Equation (7) provides an interpretation of the expected free energy as a sum of two terms. The former is the Kullback-Leibler divergence between (approximate) posterior and prior over the outcomes; it constitutes the quality score's *pragmatic* (or utility-maximizing) component, favouring policies that realise expected outcomes under the generative model. The latter is the expected entropy under the posterior over hidden states; it represents the quality score's *epistemic* (or ambiguity-minimizing) component, favouring policies that realise unambiguous outcomes. In other words, the former (pragmatic) term represents the *risk* that the anticipated outcomes $Q(o_\tau | \pi)$ diverge from prior preferences $P(o_\tau)$, while the latter (epistemic) minimises *ambiguity*. In summary, risk measures the difference between predicted and preferred outcomes \mathbf{o}_τ^π in the future, while ambiguity quantifies to what extent a future state \mathbf{s}_τ^π diminishes uncertainty about future outcomes. From a machine learning perspective, this would be equivalent to saying that \mathbf{G}_π embodies a “regularisation” term, which balances between exploitive (pragmatic) and exploratory (epistemic) behaviour.

A complementary perspective on decompositions of expected free energy is that prior preferences furnish constraints on information seeking behaviour. In other words, the expected free energy can also be expressed as expected information gain and expected value, where value is the logarithm of prior preferences in equation 7 (see penultimate equality). This reading reflects the dual optimality aspects of active inference; namely, compliance with the principles of optimal Bayesian design and decision theory, respectively. On this view, information seeking behaviour is limited to policies that portend expected value.

The expected free energy of a policy \mathbf{G}_π can be expressed in terms of linear algebra by considering the equations for the free energy minimising sufficient statistics above, together with the generative model:

$$G(\pi, \tau) = \mathbf{o}_\tau^\pi \cdot (\ln \mathbf{o}_\tau^\pi - \ln P(o_\tau)) + \mathbf{s}_\tau^\pi \cdot \mathbf{H} \quad (8)$$

with

$$\mathbf{s}_\tau^\pi = \mathbf{B}(u_\tau = \pi^{(\tau)}) \cdot \mathbf{s}_\tau$$

$$\mathbf{o}_\tau^\pi = \mathbf{A} \cdot \mathbf{s}_\tau^\pi \quad (9)$$

$$\ln P(o_\tau) = \ln \mathbf{C}$$

$$\mathbf{H} = -\text{diag}(\mathbf{A} \cdot \ln \mathbf{A})$$

where $\ln P(o_\tau)$ is the log-vector of preferred outcomes, and \mathbf{H} is the entropy matrix pertaining to future outcomes. This provides a convenient way to evaluate a policy's expected free energy.

Crucially, standard implementations of active inference assume that during action selection, an agent evaluates all its policies π for any possible future state an agent could be in. This means computing the expected free energy G_π of each policy π . Once every plausible (i.e., allowable) policy has been scored (and its associated “quality” value is evaluated), the agent uses a Boltzmann distribution to select the best policy from which the next action is sampled. Hence, in active inference, an action results from an inferential process that scores possible futures and selects the most likely policy under prior beliefs about the consequences of the action.

Active inference has been used to address a variety of cognitive phenomena, including decision-making (K. Friston et al., 2013; K. J. Friston et al., 2014), habitual behaviour, salience and curiosity-driven planning (K. J. Friston, FitzGerald, Rigoli, Schwartenbeck, O’Doherty, et al., 2016; Maisto et al., 2019; Parr & Friston, 2017; Schwartenbeck et al., 2019) and, in general, to develop a process theory for neural computation (K. J. Friston, FitzGerald, Rigoli, Schwartenbeck, & Pezzulo, 2016; Schwartenbeck et al., 2014). However, with a few exceptions (Champion et al., 2022; Fountas et al., 2020; Millidge, 2019b; Ueltzhöffer, 2018), current active inference approaches evaluate all policies exhaustively, rendering them unable to solve large POMDP problems. To fill this gap, we introduce Active Inference Tree Search below.

3. Active Inference Tree Search

A straightforward method to overcome the limitations of active inference in large POMDPs is to elude the exhaustive evaluation of all allowable policies using a heuristic procedure (Tschantz et al., 2019) (Millidge, 2019a). The efficacy of such a proposal needs to be assessed, considering the quality of the approximation and the gains in terms of computational costs and tractability. Here, we develop and evaluate a novel tree search scheme to render active inference in large POMDPs tractable: namely, Active Inference Tree Search (AcT).

AcT solves a POMDP problem using a planning tree: an abstract structure where nodes v_τ correspond to beliefs \mathbf{x}_τ about the states reachable from the current state, where the branches represent possible actions to take to reach future states. Its goal is to estimate the posterior over control states $P(u)$ from which the best action a_t can be sampled. This estimate is obtained through simulations, which start from the current state s_t (with a related observation o_t) and proceed forward through specific branches of the decision tree, corresponding to a series of paths or histories $h_\tau = (v_t u_t, v_{t+1} u_{t+1}, \dots, v_\tau)$. The simulations approximate, statistically, the expected free energy values G of the policies $\pi \equiv (u_t, u_{t+1}, u_{t+2}, \dots)$; the larger the number of simulations, the more reliable the approximation of G . This planning process is iterated until one or more halting conditions are satisfied. The depth d of the planning tree depends on two control parameters: the discount factor δ , and the discount horizon ε . In our simulations, the maximum depth of a planning tree—and consequently the maximum number of simulations employed to generate it—is fixed by imposing $\delta^d < \varepsilon$.

Note that AcT is an algorithm to build a planning tree, not to select actions. Here, we assume that after the planning tree has been built, the agent selects an action by sampling from the distribution of

control states inferred at the root node; and executes it. At this point, the agent makes a transition to a new state and receives a new observation—and can start planning again.

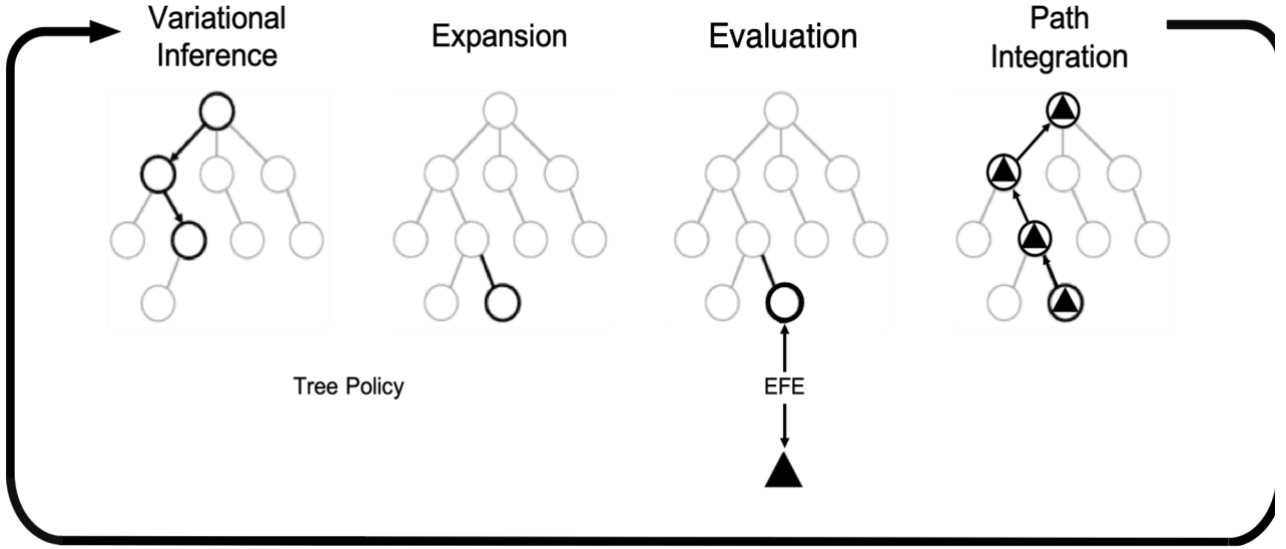


Figure 3. The four stages of the Active Inference Tree Search (AcT) algorithm. Note that the first two stages (variational inference and expansion) could be considered as two parts of a single TreePolicy procedure of MCTS (Browne et al., 2012). The third (evaluation) and the fourth (path integration) stages could be called Eval and PathIntegration procedures, respectively. The third (evaluation) stage can also be called an Eval procedure. See the main text for an illustration of each of the four stages.

3.1 The four stages of Active Inference Tree Search

Active Inference Tree Search comprises four successive stages—Variational Inference, Expansion, Evaluation, and Path Integration—applied iteratively at each time step t (Figure 3). In the following, we examine each stage in detail. Furthermore, in the Appendix, we report the pseudocode of the AcT algorithm as a function of the parameters (**A**, **B**, **C**, **D**) commonly adopted in active inference (K. Friston et al., 2015)(K. Friston et al., 2017) and of the discount factor δ widely adopted in Monte Carlo Tree Search (Kocsis & Szepesvári, 2006)(Kocsis et al., 2006).

3.1.1 First stage: Variational Inference

The goal of the first (variational inference) stage is to select the next non-terminal leaf node v_τ of the tree to expand. From the root—and recursively until reaching an expandable node of the planning tree—this stage samples an action over a Boltzmann distribution $\sigma\left(\kappa_p \ln \mathbf{E} - \gamma_\tau \cdot G(\pi_\tau, v_\tau)\right)$ that depends on three terms: 1) the EFE $G(\pi_\tau, v_\tau) = (\mathbf{A} \cdot \mathbf{x}_\tau) \cdot (\ln(\mathbf{A} \cdot \mathbf{x}_\tau) - \ln \mathbf{C}) + \mathbf{x}_\tau \cdot (\sum_i \mathbf{A}_{ij} \ln \mathbf{A}_{ij})_j$, defined in Equations (8) and (9), of the policy π_τ assembled so far, 2) the precision γ_τ computed at each depth of the tree visit, and 3) the prior belief about the policy \mathbf{E} (Parr & Friston, 2018).

Taken together, these three terms define the estimated quality of a policy and consider 1) the divergence between preferences encoded in \mathbf{C} and the expected outcomes $\mathbf{A} \cdot \mathbf{x}_\tau$, and expected entropy of observations (respectively, first and second terms of $G(\pi_\tau, v_\tau)$), 2) a modulation of the policy quality distribution that controls the stochasticity of action selection, and 3) a confidence bound that regulates exploration.

The latter term (\mathbf{E}) is modulated by a factor κ_p named *exploration factor* and is closely related to the factor c_p in the UCB1 algorithm for the Multi-armed Bandits (Auer et al., 2002)(Kuleshov & Precup, 2014). It takes the form of probabilistic distribution $\mathbf{E} \sim \sqrt{2 \ln N(v)/N(v')}$, where v' denotes a child node, $N(v')$ denotes the number of visits of v' , and $N(v)$ denotes the number of visits of the parent node v . Given this definition of \mathbf{E} , the probability of every child node decreases if it is visited frequently (i.e., with high $N(v')$) and increases when its number of visits is sufficiently lower than that of the other children (i.e., a large ratio $\ln N(v)/N(v')$). Therefore, analogous to the UCT algorithm (Kocsis & Szepesvári, 2006)(Kocsis et al., 2006), the Variational Inference stage may select every node with a probability different from zero which increases in time for less visited states. In active inference, this extra parameter is usually read as encoding prior beliefs about policies that have become habitual (i.e., habitual priors combined with empirical priors furnished by the expected free energy).

3.1.2 Second stage: Expansion

The goal of the second (expansion) stage is to expand the non-terminal leaf node v_τ selected during the former (variational inference) stage. Expansion of a leaf node v_τ corresponds to instantiating a new child node v' by implementing a random action u' among those previously unused. Each of these children stands for a future state \mathbf{x}' an agent can visit, according to the transitions defined in the matrix \mathbf{B} . By adopting a Bayesian terminology, expanding could mean defining new predictable events over the space of future policies, thereby expanding the horizon of possible events. Note that the first (variational inference) and the second (expansion) stages return the same output—a node—but the former stage *selects* a node, whereas the latter *creates* a node. It would also be possible to merge these two stages into a unique stage, analogous to TreePolicy (Browne et al., 2012) in MCTS. In Bayesian statistics, this is not unlike the procedures implicit in nonparametric Bayes, based upon stick-breaking processes that allow for an expansion of latent states (Teh et al., 2006).

3.1.3 Third stage: Evaluation

The goal of the third (evaluation) stage is to assign a value to the leaf node v_τ expanded in the previous phase. The evaluation considers the expected free energy $G(*, v_\tau)$, which is a function of the state and the observation associated with v_τ . Note that $G(*, v_\tau)$ scores the EFE of the node v_τ , not the sum of the EFEs of all the nodes from the root to the node v_τ . The EFE is then weighted by its ‘temporal precision’: a discounted factor equal to δ^τ that depends on an arbitrary parameter δ and the depth τ of the tree node v_τ . The resulting $G_\Delta = \delta^\tau \cdot G(*, v_\tau)$ value, denoted as ‘predictive EFE’, is finally assigned to v_τ . Please note that, unlike the original MCTS algorithm, evaluating the quality of nodes does not require random policies (or rollouts). This is because the EFE functional permits simultaneously estimating both the exploitive and the explorative (epistemic) value of the node.

3.1.4 Fourth stage: Path Integration

The fourth (path integration) stage aims to adjust the \mathbf{G} values of the tree nodes up to the root node v_t by considering the new values obtained during the third (Evaluation) stage. The value estimated by the Evaluation stage is used to update the quality G and the number of visits N of the nodes on the tree path v_τ, \dots, v_t obtained during the two phases of variational inference and expansion (which jointly form the TreePolicy procedure). Such updating is the statistical analogue of “path-integration” formulations in active inference (K. Friston et al., 2015), where one sums up the expected free energy at each time step in the future.

The four stages are repeated iteratively until a criterion is met to provide estimates of the \mathbf{G} values of a o tree node subnet.

3.2 Computational resources required by Active Tree Search

Most on-line planning algorithms employ a belief tree like the one shown in Figure 1, to encode the POMDP problem in a manageable form. The on-line algorithms implement multiple lookahead visits on the tree to plan the next action to execute. A belief tree of depth D contains $\mathcal{O}(|U|^D |Z|^D)$ nodes where $|U|$ and $|Z|$ are the cardinalities of the action and observation set, respectively; as a consequence, the tree size influences the performance of every algorithm relying on belief tree visits in their planning phase. For example, the popular POMCP algorithm (Silver & Veness, 2010), which grandfathers the algorithms based on tree visit sampling, is prone to this complexity. The R-DESPOT algorithm (Ye et al., 2017) generates a subtree of the belief tree of size $\mathcal{O}(|U|^D K)$ that encompasses the executions of all policies by K abstract simulations called *scenarios*. In contrast, AcT works on trees with $\mathcal{O}(|U|^D)$ nodes—of considerably less complexity—but uses lossless probabilistic representations for beliefs and observations. This requires greater memory resources and longer updating operations during the run. On the other hand, as noted in (Ye et al., 2017), POMCP and R-DESPOT, which approximate belief states and outcomes with a particle filter, have problems dealing with large observation spaces, because beliefs could collapse into single particles, causing convergence to suboptimal policies.

The total computational cost of AcT depends on the number of simulations controlled through the discount condition $\delta^d < \varepsilon$, and on the EFE computation in the Evaluation routine, which is computationally expensive. It requires a number of floating-point operations proportional to the size of the generative model (e.g., the number of hidden states $|S|$ times the number of outcomes $|O|$). Note that it would be possible to approximate or amortise EFE computations to reduce computational demands. Exploring approximations to EFE is beyond the scope of this article.

4. Results of the simulations using Active Inference Tree Search

We tested the Active Inference Tree Search on three exemplar problems. The first two problems (a deceptive binary tree and a non Lipschitzian function) exemplify deceptive “traps” that are known to challenge UCT and similar algorithms. The notion of “trap” is used in adversarial games strategy

search (Nau, 1982) to indicate those states of a game whose instantaneous utility is deceptive, with respect to their future outcomes. The third problem is a POMDP benchmark, the *RockSample* (Smith & Simmons, 2004), which is often used to evaluate the effectiveness and scalability of planning algorithms as the problem complexity increases¹.

4.1 Active Inference Tree Search avoids traps in deceptive binary trees

Ramanujan et al. (Ramanujan et al., 2010) noted that the performance of the UCT algorithm is limited in games where the best proximal decisions do not necessarily correspond to winning strategies. This is the case, for example, in chess, where exhaustive search (e.g., minimax) yields better performance than sampling-based approaches. This is due to particular game configurations in which an unfortunate move unavoidably leads to a defeat. These game states are called *traps* because, as noticed above, their instantaneous utility is deceptive with respect to the future outcomes that they lead to. Being able to escape from traps is a crucial feature of successful planning algorithms.

Coquelin & Munos (Coquelin & Munos, 2014) introduced an example challenging problem for sampling-based planning algorithms. This problem has just two actions, $2D + 1$ states parameterised by $D \in \mathbb{N}$, and deterministic rewards. At each time step d , one can get a reward of $(D - d)/D$ by choosing action 2; alternatively, one can move forward by choosing action 1. At time $D - 1$, action 1 corresponds to an absorbing state with maximum reward 1 and action 2 to another absorbing state with reward 0. Intuitively, the state space of the problem can be described as a binary tree of depth D (Figure 4). The optimal plan involves always selecting action 1, to move along all the branch levels d and reach the final (maximum) reward. Finding this solution is challenging for sampling methods, as the suboptimal action 2 is much more rewarding in the proximity of the root—and this immediate reward influences planning following the first moves. Coquelin & Munos proved by induction that UCT has a hyper-exponential dependency concerning the depth D of the binary tree. Considering the worst case, it takes $\Omega(\exp(\dots(\exp(1))\dots))$ – composed by $D - 1$ exponential functions to get the reward¹.

To check whether AcT suffers the same limitation, we compared UCT, AcT, and a reduced version of AcT, called FE, which does not use the policy prior beliefs \mathbf{E} during the exploration stage (or, analogously, with $\kappa_p = 0$). To render this problem suitable for AcT, we reformulated it as an MDP problem, i.e., a Markov Decision Problem that is fully observable. The MDP comprises $2D + 1$ hidden states, a corresponding set of $2D + 1$ observations (consequently \mathbf{A} is diagonal), action “1” and “2” to move from one state to another (reported in \mathbf{B}) and a vector \mathbf{C} where rewards are spread over observations by a probabilistic distribution encoding preferences.

¹ Our simulations are carried out by using a C++ implementation of AcT as a header library developed by us. The library implements a multicore parallelisation of the most demanding computational kernels. Note that most of the computational complexity of AcT depends on the multidimensional inner products involved both in EFE computation and state estimation.

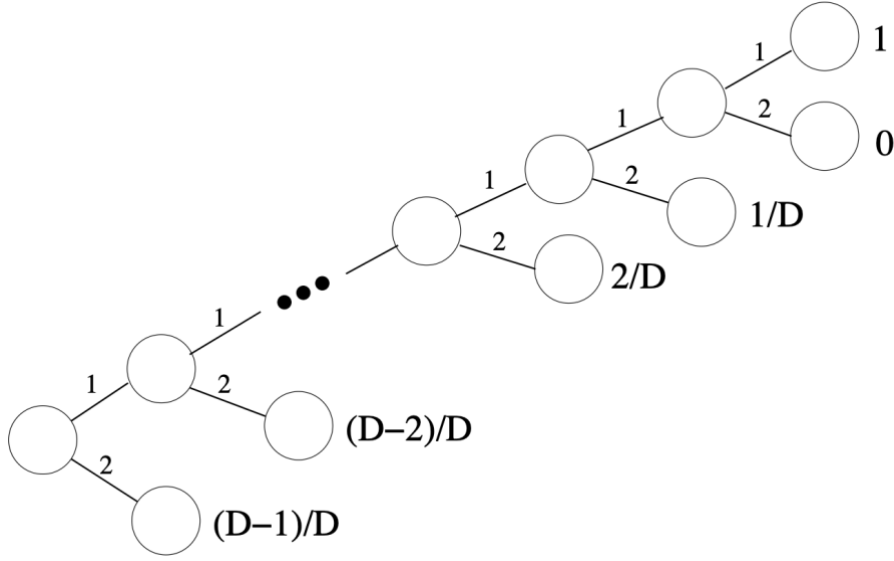
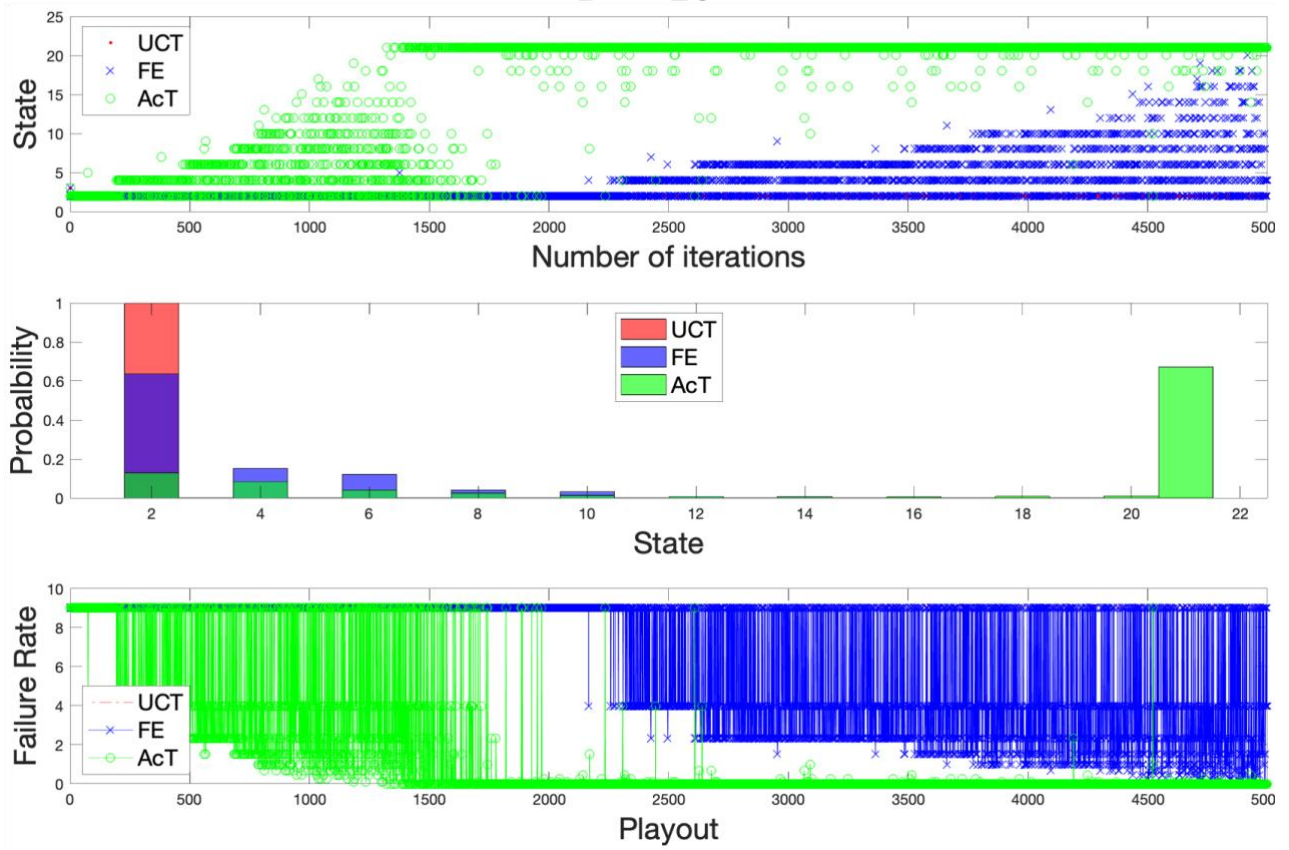


Figure 4. A binary tree representing the state space of a challenging problem for sampling-based planning methods (adapted from (Coquelin & Munos, 2014)). From the root (left node) toward the deepest level D , action 2 at each level leads to a deceptive leaf node with reward $(D - d)/D$. The optimal policy involves always selecting action 1, which yields reward 1.

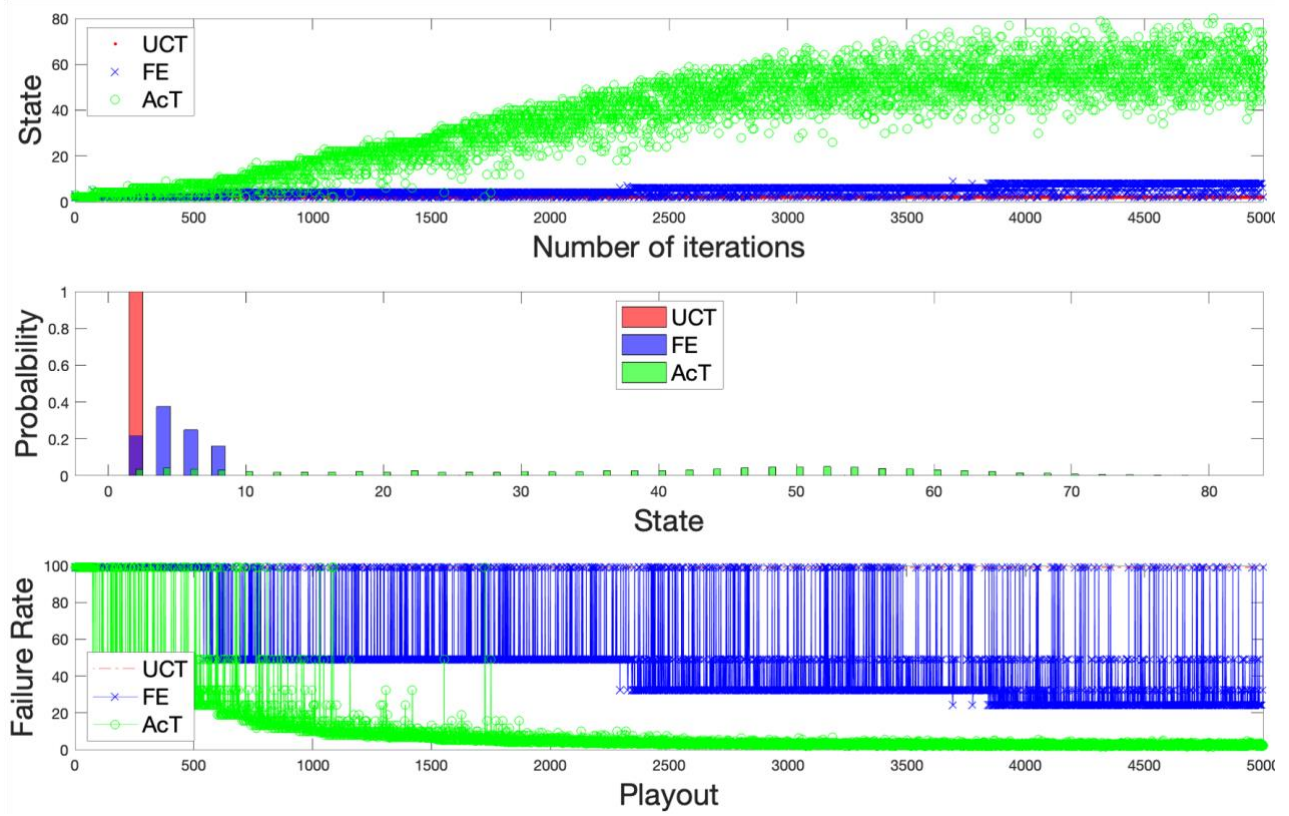
We considered three problems of increasing depth: $D = 10$, 100, and 1000. For each problem, we collected the results of 1000 executions of the three algorithms (UCT, AcT and FE) using a fixed number of simulations or playouts (5000). We used a discount factor of $\delta = 0.95$, and set the exploration parameter $\kappa_p = 1$ for both UCT and AcT. The results are shown in Figure 5 by plotting—for each algorithm—the modes of the occupied states, the occupancy probabilities, and the failure rate (defined as the relative difference between the depth d of the visited state and D), as a function of the simulation number.

Our results show that UCT experiences problems starting from $D = 10$ selecting the first deceptive states. Conversely, both algorithms using active inference reached the deepest state, despite performance decreases with greater D . FE exhibits a more pronounced greedy behaviour. At the same time, AcT keeps exploring due to the prior distribution **E**. This numerical analysis suggests that AcT has the best performance: compared to the other algorithms—it reaches deeper states of the deceptive tree and does so faster.

$D = 10$



$D = 100$



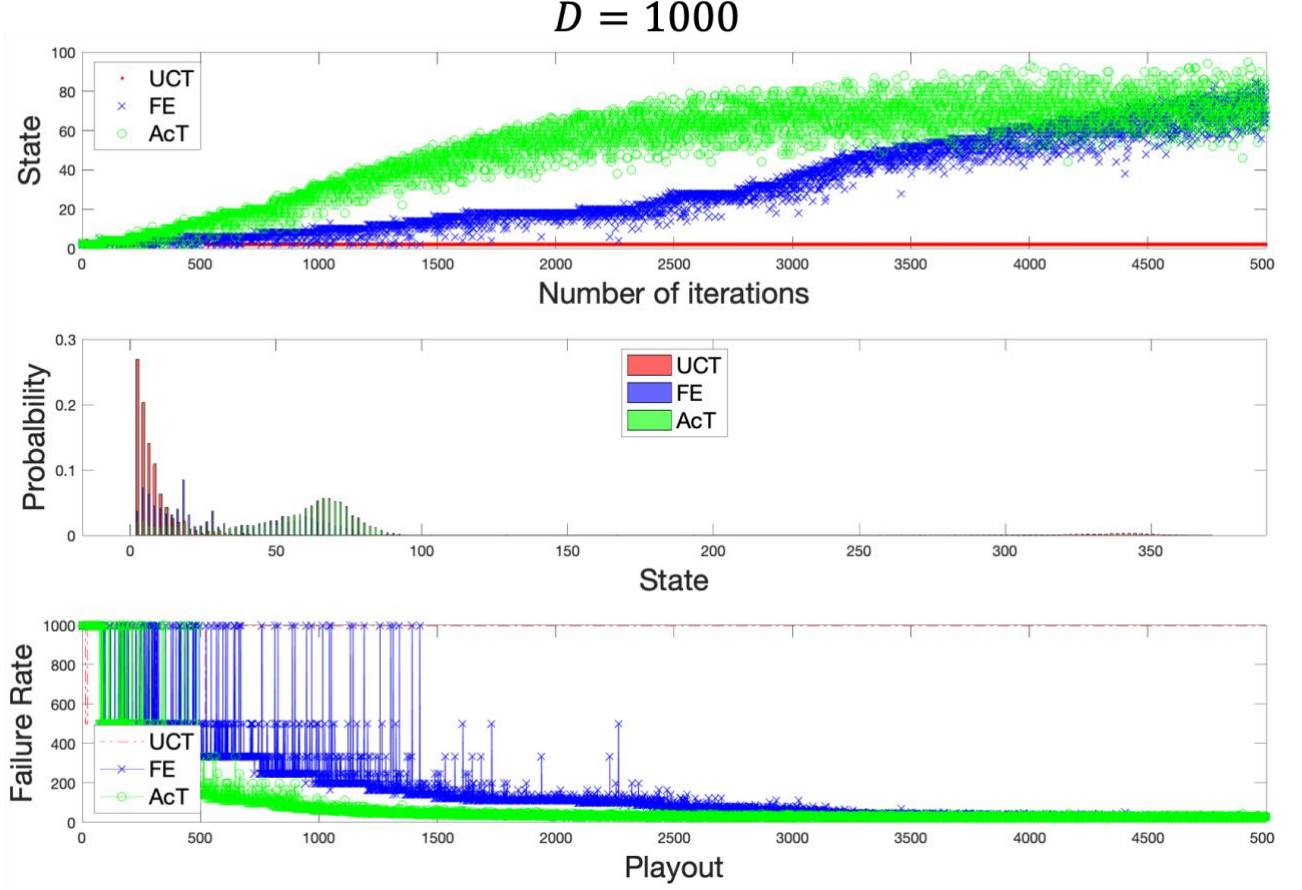


Figure 5. Experimental results in the deceptive binary tree of (Coquelin & Munos, 2014) of depths $D = 10, 100, 100$ (top, middle, and bottom panels, respectively). Each panel plots state occupation (top), occupation probability (middle), and failure rate (bottom) as a function of the number of simulations (or playouts).

4.2 Active Inference Tree Search reaches an adaptive level of exploration when finding the global maximum of a non Lipschitzian function

The above problem can be considered illustrative of a whole class of MDP domains on which sampling algorithms manifest shortcomings (Steven et al., 2017). These problems are all characterised by the lack of smoothness of the objective or value function, where the notion of “smoothness” corresponds to a well-behaved analytic or continuous value function. Formally, this condition can be expressed through the Lipschitz continuity, according to which a value function $V(s)$ defined over the state-space S is M -Lipschitz continuous if $\forall s_1, s_2 \in S, |V(s_1) - V(s_2)| \leq M \|k(s_1) - k(s_2)\|$, where M is a constant and $k(\cdot)$ is a mapping from S to some normed vector space (Pazis & Parr, 2011). The challenge for any optimisation scheme is to find the global maximum of a non-Lipschitzian function. The function:

$$g(x) = \begin{cases} 0.5 + 0.5 \left| \sin \frac{1}{x^5} \right|, & 0 < x < 0.5 \\ 0.35 + 0.5 \left| \sin \frac{1}{x^5} \right|, & 0.5 \leq x \leq 1 \end{cases} \quad (10)$$

introduced as a test in (Steven et al., 2017), has two distinct behaviours over its domain (see panel A in Figure 6). In the (left) interval $[0, 0.5]$, there exist numerous global optima, but their functional form is quite rough, whereby in the (right) interval $[0.5, 1]$, the function is smooth, but the extrema are suboptimal. In this case, an effective search algorithm should explore every domain region.

As for the binary-tree test used before, we cast this optimisation problem as MDP problem: each state represents some interval $[a, b]$ within this unit square, with the starting state representing $[0, 1]$. We assume that there are two available actions at each state, the former resulting in a transition to the new state $[a, (b - a)/2]$ and the second resulting in a transition to $[(b - a)/2, b]$. For example, at the starting state, the agent has the choice between a "left" action to make a transition to the state $[0, 0.5]$ and a "right" action to make a transition to the state $[0.5, 1]$. After it selects the left action, it has a choice between another "left" action to make a transition to $[0, 0.25]$ or a "right" action to $[0.25, 0.5]$, and so on. Consequently, with increasingly deeper planning trees, the agent explores more fine-grained intervals. An efficient planner should visit the left interval $[0, 0.5]$ extensively and deeply (i.e., approach zero), as it encompasses many maxima.

The state-space S can be represented as a binary tree whose depth is constrained by a trade-off set by the condition $b - a < 10^{-5}$. Transitions between states, which move from a state s at a depth d of the binary tree to a state s' at depth $d + 1$ are controlled through the matrix B . Analogous to the function " g " shown in Equation 10, also the transition function $s' = B(s, u, t)$ is Lipschitzian but only for domain values larger than 0.5. This is evident by plotting (Figure 6, panel B) the Lipschitzian constant M averaged over all the transitions between two consecutive depths, for $x < 0.5$ and for $x > 0.5$ (blue and red lines, respectively). For $x \in [0.5, 1]$, M increases until it reaches the upper bound value of 10 (for $d > 10$). Instead, for $x \in [0, 0.5]$, M shows an exponential behaviour and rapidly reaches much greater values. Each state corresponds to one observation, resulting in an MDP where the matrix A is diagonal. The a priori distribution C is computed empirically by considering the value of $g(x)$ in the midpoint of the domain interval encoded by the states. The discount factor δ was set to 0.95.

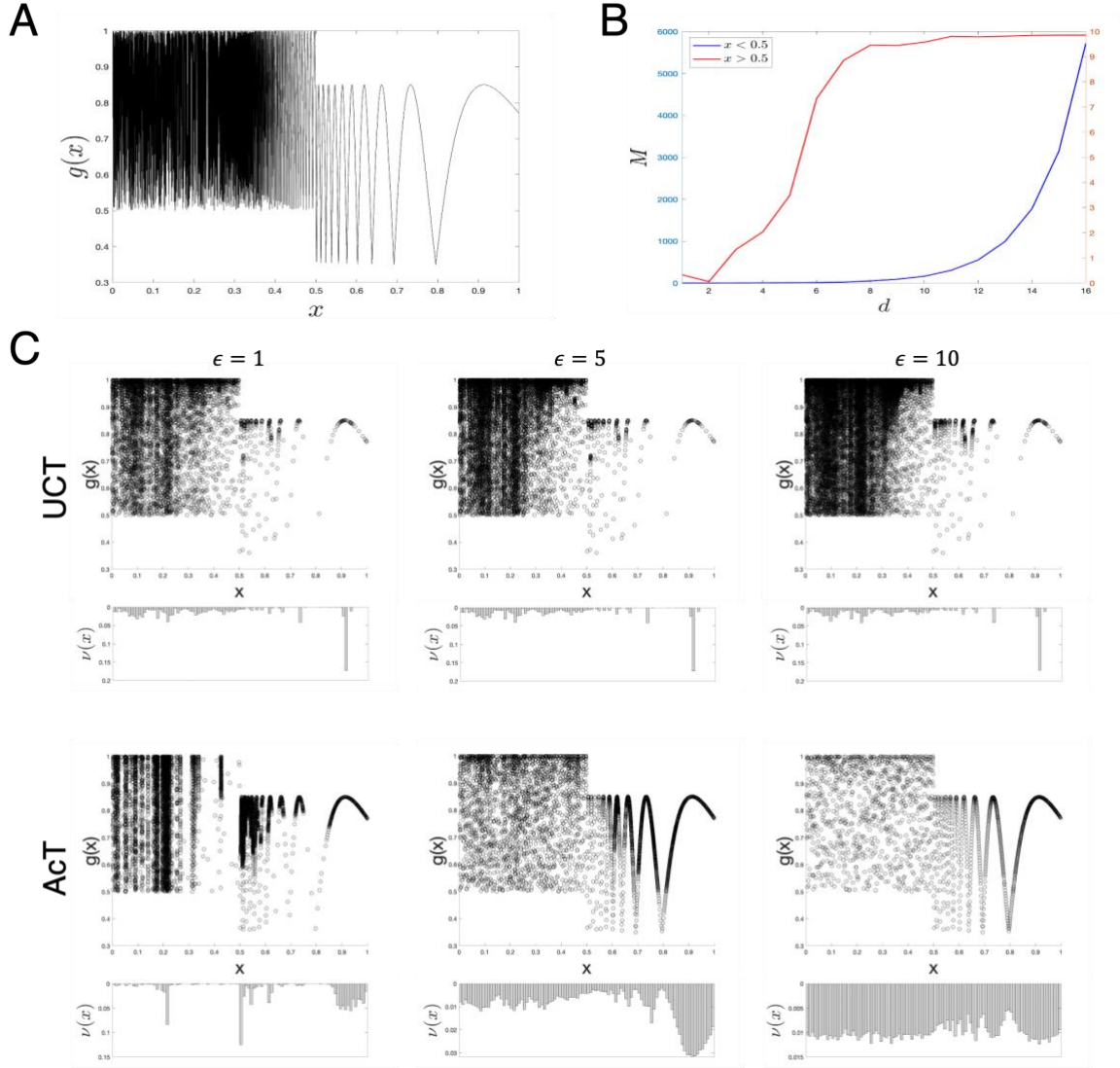


Figure 6. The function “ g ” used to test the efficacy of the AcT and UCT algorithms in problems with a rough landscape. A) “ g ” function defined in $[0,1]$ is Lipschitz-continuous for values larger than 0.5, yet it is not otherwise. B) The average value of the Lipschitz constant M over all the state transitions at a given depth of the binary tree used to encode the optimisation problem as MDP. The red curve is for $x \in [0.5,1]$, whereas the blue plot is for $x \in [0,0.5]$. C) A matrix plot whose elements are the scatter plots of the values encoded by the node states visited by UCT and AcT (1000 executions each); the bottom parts show the histograms $\nu(x)$ of their domain values. The matrix plot arranges the rows by the algorithm (first row for UCT, second row for AcT) and columns according to the values of the exploration factor κ_p set for the executions.

We compared the UCT and AcT algorithms, for 1000 executions each, with three levels of the exploration factor κ_p ($\kappa_p = 1, 5, 10$). Unlike (Steven et al., 2017), we found that UCT explores the whole domain of g , although it mostly visits a state corresponding to an x value around 0.9; see the element (1,1) of the matrix of plots in Figure 6C. AcT explores deeper parts of the tree search (plot (2,1) in Figure 6C) and is able to find maxima in the whole domain of g . Compared to UCT, AcT

shows greater exploitative behaviour in correspondence with specific significant x values, for instance, 0.5, 0.9, and 0.2 (that are the modes of the visited x distributions).

This optimisation problem illustrates the effects of the exploration factor κ_p on algorithm performance. Reading Figure 6C out by columns, one can evaluate the effects of κ_p on the algorithms UCT (first row) and AcT (second row). The performance of UCT remains relatively stable across all the values of ϵ , in the sense that despite the increase of exploration with greater values of κ_p , the statistical distribution $v(x)$ of the visited domain points remains unchanged. Instead, the effects of the parameter ϵ on AcT are more significant. For $\kappa_p = 1$, AcT shows limited exploration, similar to the FE algorithm used in the deceptive binary tree example. This is because, in this particular problem, the term used to sample the actions (related to the \mathbf{E} and controlled by κ_p) is numerically much smaller than the one related to the policy value \mathbf{G} . When ϵ is set to 5 or 10, AcT explores significantly more and (with $\kappa_p = 10$) it visits the g codomain uniformly. In this latter case, AcT also visits the unrewarded branches of the binary tree, even if this implies a reduction of performance; this becomes apparent by noticing that $v(x)$ is almost flat for $\kappa_p = 10$.

4.3 Active Tree Search in large POMDP problems: the case of *RockSample*

RockSample(n, k) (Smith & Simmons, 2004) is a well-known benchmark problem for assessing POMDP solvers and their scalability. It simulates a rover whose task is collecting *samples* of k scientifically valuable rocks deployed on an $n \times n$ alien soil grid—and then leaving the area. Samples come in two varieties: valuable or invaluable. The rover earns a reward for each valuable sample it collects and a penalty for each invaluable sample. The rover knows the locations of the rocks but can only evaluate whether they are valuable via a long-range sensor, whose measures are affected by an error, which increases exponentially with the distance between the rover and the rock examined. We considered two variants of this problem, with (n, k) equal to (7,8) and to (11,11).

Representing this problem in a format suitable for active inference is straightforward. In principle, the problem state space S can be factorised to reduce the total number of states (Ong et al., 2009). Still, we decided to retain both variants without factorised representations to leverage the problem's difficulty. Therefore, the cardinality of the state space is $|S| = n^2 * 2^k + 1$ (12,544 in the case (7,8) and 247,808 in (11,11)), necessary to encode every possible combination of locations and the scientific value of the rocks plus an additional “exit” state. This cardinality is needed to define the initial belief state \mathbf{D} and the transition state matrix \mathbf{B} , which is also conditioned on the control state (actions) $a \in U$ that the agent can make.

The set U contains the four actions (go north, go south, go east, go west) that the agent uses to move around the square, k actions that the agent uses to evaluate the rocks remotely (one action for each rock), and a sampling action to collect a rock sample. Observations are factorised into three factors, which relate to the positions on the grid, the configuration (2^k) encoding the scientific quality of the rocks, and their associated rewards, respectively. Accordingly, the likelihood \mathbf{A} is decomposed into three factors, each one encoded as a cubic matrix (generally as a tensor when the state space, in turn, is subdivided into factors), where the first dimension represents the observations, the second the states, and the last the actions. Introducing a dependency of \mathbf{A} on the actions is uncommon in active

inference but useful in many POMDP problems, including $RockSample(n, k)$. This is because the observation one gets by sampling a rock (with an action k) is a function of the distance from the rock; encoding this contingency would require a considerable number of states if one does not express \mathbf{A} as a function of actions. Reward contingencies expressed in \mathbf{A} are action-dependent, too, as the agent obtains a “good” observation when it samples a good rock (and a “bad” observation otherwise)—and when it exits the game. Finally, \mathbf{C} encodes preferred observations and comprises three modalities: in the first two, observations are uniformly preferred, while in the last they are drawn from a Bernoulli distribution, with a success probability almost equal to 1. See the Appendix for an example generative model for $RockSample$, with $n = 2$ and $k = 1$.

We used the same parameters for both $RockSample(7,8)$ and $RockSample(11,11)$. We used a discount factor δ equal to 0.95 and a ‘discount horizon’ ε of 0.4 so that the depth d of the tree search developed during planning is about 19 steps (a threshold computed by considering that $\delta^d < \varepsilon$). We evaluated 1000 executions of AcT, with different seeds from a pseudorandom number generator and with different (random) arrangements of rocks in the grid.

In keeping with previous works (Silver & Veness, 2010)(Ye et al., 2017), we augmented the AcT algorithm with a domain-specific, heuristic policy that prioritises some selected actions during the simulations. Specifically, the heuristic policy prioritises actions that approach the rocks with more “good” observations and actions that check rocks with uncertain outcomes (ensuing from inconsistent observations). When the rover is in the same place as a rock evaluated as “good” by most observations, the heuristic policy prioritises sampling actions. Finally, when all the rocks in the scenario have been sampled, the heuristic policy prioritises actions heading toward the exit.

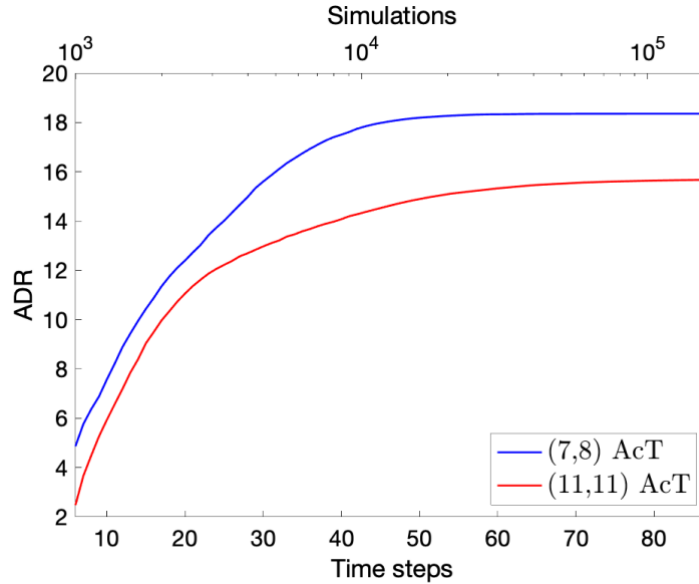


Figure 7. Total discounted reward achieved by the AcT algorithm augmented with the heuristic policy for $RockSample(7,8)$ and $RockSample(11,11)$ (in blue and red, respectively). Results are shown as a function of the time steps (at the bottom axis) and the number of simulations (in logarithmic scale, top axis). All results are averaged over 1000 executions.

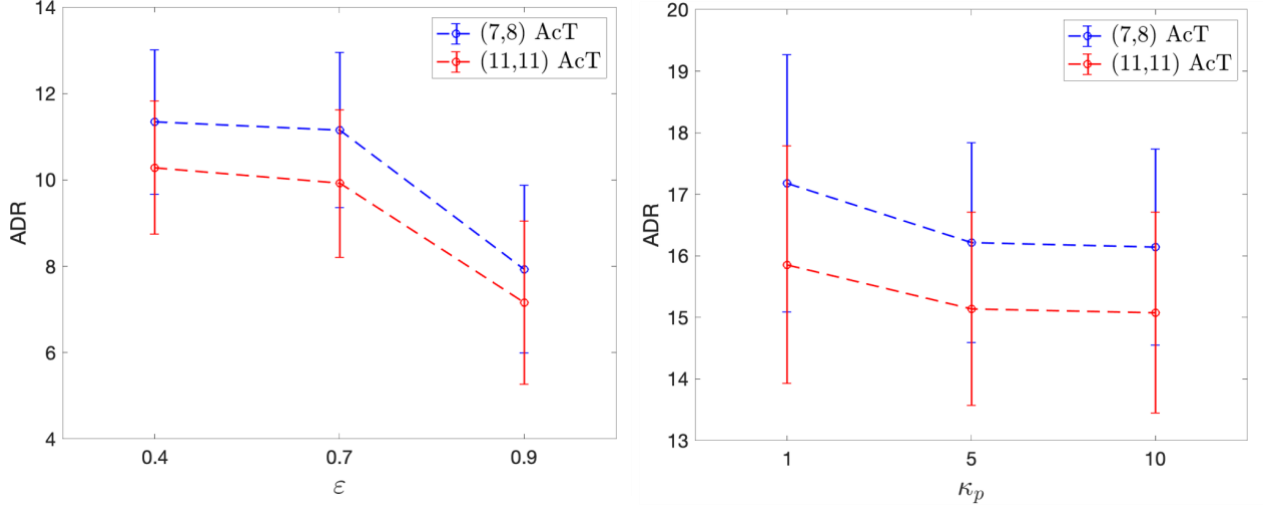


Figure 8. Total discounted reward (ADR) averaged over 1000 execution, obtained by AcT as a function of its control parameters. Left panel: ADR as a function of the discount horizon ε (with $\kappa_p = 1$). Right panel: ADR as a function of the exploration factor κ_p (with $\varepsilon = 0.4$). In both panels, the blue and the red lines represent the results obtained for *RockSample*(7,8) and *RockSample*(11,11), respectively.

Figure 7 shows the model performance, expressed as the total discounted reward (ADR) $\bar{R}_t^\delta = \frac{1}{N} \sum_{i=1}^N \sum_{\tau=0}^t \delta^\tau r_i(\tau)$ averaged over N executions, as a function of time steps t required to complete the task. In *RockSample*(7,8), AcT achieves 18.35 ± 4.17 ADR in 38.92 time steps and 52,672.5 simulations (on average). In *RockSample*(11,11), AcT achieves 15.71 ± 3.86 ADR in 74.93 timesteps, with 238,461 simulations (on average)². In both *RockSample*(7,8) and *RockSample*(11,11), AcT scales up smoothly with the size of the problem, as evident from the fact that the algorithm's performance shows the same trend in both problems.

We analysed the performance of AcT in *RockSample*(7,8) and *RockSample*(11,11) as a function of the horizon discount parameter ε (Figure 8A). As expected, the performance of AcT decreases when ε increases (and consequently, the maximum depth of the planning trees decreases). It could be noted that there is a threshold (which is plausibly domain-specific), after which the increase of ε becomes catastrophic. Indeed, AcT preserves its effectiveness between $\varepsilon = 0.4$ and $\varepsilon = 0.7$ but becomes unsuccessful with $\varepsilon = 0.9$ when the planning tree becomes excessively small.

² The AcT algorithm without the domain-specific heuristic policy achieves significantly lower scores: 13.4251 ± 5.89 ADR for *RockSample*(7,8) with $\varepsilon = 0.7$, and 6.15488 ± 3.82329 ADR for *RockSample*(11,11) with $\varepsilon = 0.9$. Please note that these results are obtained with ε values significantly higher than those reported in the main simulation ($\varepsilon = 0.4$). This is because using $\varepsilon = 0.4$ without the heuristic policy entails significant memory demands. Increasing ε permits decreasing memory demands by constraining the depth of the planning tree.

Furthermore, we analysed the performance of AcT in *RockSample*(7,8) and *RockSample*(11,11) as a function of the exploration factor κ_p (Figure 8B), while keeping the horizon discount parameter ε fixed ($\varepsilon = 0.4$). The performance of AcT decreases when the exploration factor κ_p is increased from 1 to 5 or 10 (the results for $\kappa_p = 5$ and $\kappa_p = 10$ are almost indistinguishable). This result indicates that an explorative approach is ineffective in *RockSample*, as it leads AcT to overextend the tree width, disregarding the most rewarding branches.

Finally, we compared the performance of AcT with state-of-the-art (on-line and off-line) POMDP algorithms, as reported in (Ye et al., 2017); see Table 1. These include: SARSOP (Spaan & Vlassis, 2005), one of the fastest off-line POMDP algorithms, with good results (often better than on-line algorithms) on POMDPs of moderate size but with severe limits in terms of scalability; AEMS2 (Shani et al., 2013), one of the early on-line algorithm not explicitly designed for very large state POMDP problems; POMCP, a widely known on-line algorithm based on Monte Carlo Tree Search designed to face with highly large-scale domains; and DESPOT (Ye et al., 2017), which is widely considered as the best performing on-line algorithm on extreme size problems.

<i>RockSample</i>	$ S ; U $	AcT	AEMS2	SARSOP	POMCP	DESPOT
(7,8)	12,544 ; 13	18.55 ± 4.32	20.89 ± 0.30	21.47 ± 0.04	16.80 ± 0.30	20.93 ± 0.30
(11,11)	247,808 ; 16	15.84 ± 4.01	—	21.56 ± 0.11	18.64 ± 0.28	21.75 ± 0.30

Table 1. Comparison of the performance of AcT and a representative set of the state-of-the-art (on-line and off-line) POMDP algorithms in *RockSample*(7,8) and *RockSample*(11,11). All the reported values (except AcT) are taken from (Ye et al., 2017).

Our results show that the performance of AcT is comparable with (but slightly lower than) state-of-art POMDP algorithms. However, it is worth considering that there are foundational differences between AcT and the other algorithms, which complicate the use of the ADR as a performance measure. First, the POMDP algorithms considered here are specifically designed to optimise exactly the (total discounted reward, ADR) score that is used for the evaluation. In contrast, AcT does not include any discount factor. Second, the *RockSample* problem is defined as a discounted reward POMDP, which fits the requirements of the POMDP algorithms considered here. However, the generative model used by AcT does not natively use the same problem definition (e.g., it associates outcomes and rewards only to states, not to actions). While some automatic ways to transform discounted rewarded POMDP problems into a “goal POMDP” (Bonet & Geffner, 2009), no equivalent procedure exists to map them into the native formulation used in AcT. Finally, AcT is not just trying to optimise discounted reward; it is trying to do so in the context of minimising uncertainty about hidden states, i.e., maximising expected information gain and expected preferences simultaneously. Despite these differences, the performance of AcT remains largely comparable with state-of-the-art algorithms specifically developed to address the POMDP problems exemplified by *RockSample*.

In sum, the simulations reported in this section provide a proof of principle that active inference can be scaled to deep planning problems. In the next section, we consider the Active Inference Tree Search algorithm from the perspective of neuronal dynamics.

4.4 Simulated neuronal dynamics of Active Inference Tree Search

This section illustrates the usage of Active Inference Tree Search to simulate behavioural and neurophysiological responses during human planning. To exemplify this, we apply Active Inference Tree Search to “Tiger”: a popular POMDP problem introduced in (Cassandra et al., 1994), to illustrate the importance of epistemic, information-gathering actions (that aim to acquire information to reduce uncertainty) during planning. In the Tiger problem, an agent stands in front of two doors and has to decide which one to open. The agent knows that one of the two doors hides a treasure, whereas the other conceals a tiger. If the agent opens the door with the treasure, it receives a reward, but if it opens the door with the tiger, it receives a penalty. The agent does not know where the tiger is but can resolve uncertainty by “listening for animal’s noises” (which induces a small cost).

The domain of this problem is usually represented as a POMDP with 2 states (tiger behind the left or right doors), 3 actions (to open the two doors or listen), and 2 observations (reward or penalty). To ensure compatibility with previous active inference studies, we recast the problem as a T-maze with 8 states, 4 actions and 16 observations (K. Friston et al., 2015). The 8 states result from the multiplication of 4 locations times 2 hidden contexts. The 4 locations correspond to the centre (i.e., start location), the left and the right arms (analogous to the two doors, with treasure and tiger, respectively), and the lower arm (analogous to a listening location, where a cue can be found that discriminates the tiger location). The 2 hidden contexts correspond to the 2 possible reward locations (i.e., the reward at the left or the right arm, respectively). The 4 actions move the agent deterministically to each of the 4 locations (but cannot change hidden context). Finally, the 16 observations result from the multiplication of 4 positional observations (that correspond 1-to-1 to the 4 locations) by 4 outcomes (i.e., reward, penalty, cue for the tiger at left, and cue for the tiger at right) that are obtained in different states, see below.

The matrices **A**, **B**, and the vectors **C** and **D** specify the agent’s generative model. The (likelihood) matrix **A** is a probabilistic mapping from states to outcomes. It specifies that the centre location provides an ambiguous cue (i.e., a cue that is identical if the agent is in either of the 2 hidden contexts and hence does not provide any information about the reward location). Furthermore, it specifies that the lower arm provides a disambiguating cue—that discloses which of the 2 hidden contexts the agent is in (and hence the reward location). Finally, the likelihood specifies that if the agent is in the first hidden context (“reward at the right arm”), the right and the left arms provide a reward and a penalty, respectively, with probability $p = 0.90$. On the contrary, if the agent is in the second hidden context (“reward at the left”), the right and the left arms provide a penalty and a reward, respectively, with probability $p = 0.90$.

The **B**(u) (transition) matrices define 4 action-specific stochastic transitions between states. These move the agent deterministically to each of the 4 locations (but cannot change its hidden context). However, there is a peculiarity: given that the task ends when the agent is in one of the upper arms (i.e., opens one of the two doors), we consider the corresponding hidden states as absorbing states that cannot be left, whatever the action.

The vector **C** encodes the probability mass over preferred outcomes. It is determined by applying the Softmax function over a utility vector having 2 and -2 , respectively, for rewarding and penalty outcomes and zeros otherwise. Finally, **D** represents the agent's belief about its initial state. The agent knows that it starts from the centre location, but—crucially—it does not know in which of the 2 hidden contexts it is in (i.e., it does not know the reward location, left or right). This is why it is optimal for the agent to go to the lower arm to solicit a cue (i.e., "listen") that disambiguates the hidden context before deciding whether to visit the left or right arms. As in the previous simulations $\delta = 0.9$.

Figure 9 illustrates the results of Active Inference Tree Search simulations, in which the reward is in the right arm. The upper panel shows the agent's state-belief distribution over time and the true states (cyan circles). At the first epoch, the agent knows it is in the centre location but does not know its current context. This is evident when considering that in the first column of the upper panel, the belief distribution spans states 1 and 2 (i.e., centre location in the first and second hidden contexts). The agent then selects an action to visit the lower arm, to collect a cue; and it discovers that the hidden context is the first (reward at the right arm). This is evident in the second column of the upper panel, where the belief distribution is concentrated in state 7 (i.e., lower arm, first hidden context). Note that the agent decided to explore the lower arm to secure a cue, instead of guessing which of the two arms is rewarding. Although this entails a cost (a delay in reaching the reward location later), this “epistemic behaviour” ensures the selection of the rewarding arm at the next epoch, see the third column of the upper panel. This epistemic behaviour emerges automatically in active inference (K. J. Friston, 2010) because policy selection considers the expected reduction of uncertainty along with utility maximisation (see Equation (7) of the section “active inference”).

The second panel of Figure 9 shows the “search trees” that AcT generates during each epoch. The left picture of the second panel shows the search tree generated during the first epoch, where the thickness of the edges connecting levels reports the probabilities of going to one of the 4 locations. The preferred plan at depth one is to make an “epistemic” move to visit the lower arm. At depth two, the two preferred actions are to visit the lower arm and (to a lesser extent) the centre location. This is because the tree search has not yet received any observation from the generative process and therefore has no information about the tiger location—hence it avoids states that include potential penalties.

The centre graphic of the second panel shows the search tree generated during the second epoch after the agent has visited the lower arm and has observed an informative cue. At this point, the agent constructs a new search tree where the plan to reach the right arm is highly probable. The choice remains the same at the last epoch (see the right picture of the third panel), and the agent collects the rewarding outcome.

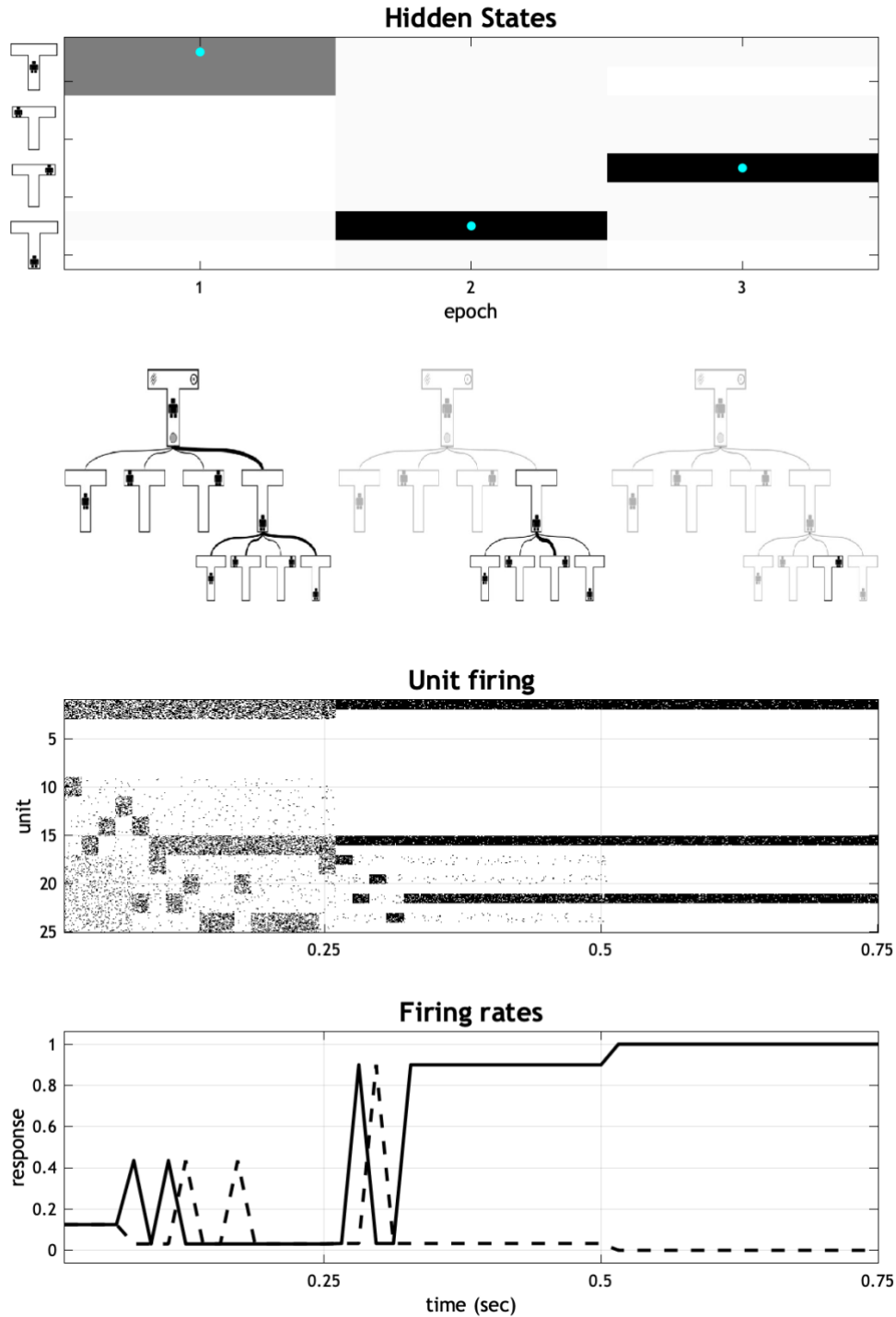


Figure 9. Simulated behavioural and neuronal responses of Active Inference Tree Search in the “Tiger” problem when the tiger is behind the left door. The first (top) panel shows the belief distribution of the eight hidden states (4 locations times 2 contexts) of the problem. The second panel illustrates the search trees generated by AcT in the three epochs of the simulation. The third panel shows simulated neurophysiological responses associated with the planning problem. These are shown as firing rates of 24 single cells that encode hidden states (8 hidden states for each of the 3 epochs) in a raster plot format. The fourth panel plots the firing rates of two units encoding the right arm (solid line) and left arm (dashed line) on the third epoch. These are the states that will be finally selected (right arm) and unselected (left arm). See the main text for an explanation.

The third panel of Figure 9 illustrates simulated neurophysiological responses during the simulation shown in the first two panels. We assume that outcomes are sampled every 250 ms: a timescale compatible with hippocampal theta cycles, where place cells representing current and prospective locations can be decoded (Foster & Wilson, 2007; Pezzulo et al., 2014; Pezzulo, Kemere, et al., 2017). The figure illustrates a raster plot of simulated neuronal activity for units encoding hidden states. The image is organised as a matrix, with 24 rows/neurons (4 locations times 2 contexts times 3 epochs, corresponding to the planning horizon) and as many columns as the number of rollouts—as implemented by AcT during the three decision epochs (16 in this simulation). In other words, the presence of 24 rows/neurons indicates that at each epoch, the agent represents its current epoch and the two closest epochs (e.g., during the first epoch, it also represents the subsequent two epochs; during the second epoch, it represents the previous and the subsequent epochs). Furthermore, separate neuronal populations encode the same hidden states at different epochs (e.g., the first hidden state at the first and second epochs correspond to the 1st and the 9th rows/neurons, respectively). In effect, this endows the agent with a form of working memory that is both predictive and postdictive.

The rows and the columns of the third panel can be grouped to cluster the matrix in 3×3 blocks of length 8 and 16, respectively. In this format, the elements shown in the main diagonal of the block matrix are beliefs about the present and correspond to the hidden states shown in the first panel. The elements shown in the upper and lower diagonal blocks correspond to (postdictive and predictive) beliefs about the past and the future, respectively. Note that the elements under the main diagonal correspond to the beliefs shown in the search trees of the second panel.

The fourth panel of Figure 9 reports the simulated firing rates of two selected units, which correspond to the states representing the left (dashed line) and the right arm (solid line) during the third epoch. These are the states that will be visited (right arm) and not visited (left arm) during the third epoch. Initially (first column of the fourth panel), both units have the same firing rates because the agent is uncertain about the state it will visit next. However, this uncertainty is resolved during the second epoch and confirmed during the third (second and third columns, respectively). It is evident from this panel that expectations about future visitations (corresponding to the firing rates of the two units) diverge during the epochs, following a stepwise evidence accumulation (K. J. Friston, FitzGerald, Rigoli, Schwartenbeck, & Pezzulo, 2016).

These simulations exemplify the possibility of establishing a mapping between algorithmic methods of AcT and neuronal processes relevant to neuroscience. For example, the neurophysiological responses shown in the last two panels of Figure 9 exemplify prospective (and retrospective) representations of states that have been consistently reported in rodents (Miller et al., 2017; Pfeiffer & Foster, 2013; Redish, 2016), monkeys (Mushiake et al., 2006; Saito et al., 2005), and humans (Kurth-Nelson et al., 2016; Schuck & Niv, 2019) engaged in a sequential decision or navigation tasks. From a cognitive science perspective, postdictive and predictive representations of this sort could be construed as working memory.

While computational modelling is widely used in neuroscience, there is still a paucity of methods that can both address large-scale problems relevant to AI and generate predictions relevant to neuroscience. Some recent studies using powerful deep learning (Storrs & Kriegeskorte, 2019; Sussillo et al., 2015; Yamins & DiCarlo, 2016) and Bayesian methods (George et al., 2017) are already bridging this gap, but they mostly address specific domains, such as visual perception and motor control. Addressing tasks such as *RockSample* or *Tiger* requires designing complete agent architectures instead, as exemplified by AcT (this paper) and deep reinforcement learning models (Botvinick et al., 2020). AcT and deep reinforcement learning models appeal to different principles—e.g., free energy minimisation versus reward maximisation; inference versus trial-and-error learning; appeal to the Bellman optimality principle versus variational principles of least action, and so on—to design agent architectures that solve complex tasks, hence speaking to different views of neuronal dynamics. Comparing the empirical validity of these assumptions side-by-side is an important objective for future research.

5. Discussion

Model-based planning is a widely interdisciplinary topic. However, synthesising ideas and methods from disciplines as diverse as AI, machine learning, and cognitive and computational neuroscience has been challenging, given their different focus (e.g., scalability and efficiency in AI, biological realism in neuroscience).

Here, we offer a significant step in this direction by extending a prominent neurobiological theory of model-based control and planning—active inference—to scale it up to POMDP problems much larger size. This extension exploits tree search to elude the extensive evaluation of action policies often countenanced in active inference. The theoretical synthesis of active inference and tree search planning methods—called *Active Inference Tree Search*—has benefits for both. On the one hand, augmenting active inference with tree search methods permits realising a novel and appealing process model for approximate planning. This renders it scalable and potentially useful for explaining bounded forms of cognition and reasoning (Huys et al., 2015; Keramati et al., 2016; Ortega & Braun, 2013; Pezzulo et al., 2013). On the other hand, active inference provides a theoretically motivated and biologically grounded framework to balance exploration and exploitation, which contextualises heuristic methods widely adopted in tree search planning, permits avoiding rollouts (as in Monte-Carlo methods) and obtains remarkable results in challenging POMDP problems.

We validated *Active Inference Tree Search* in three simulative studies. The first study's results show that AcT successfully addresses deceptive binary trees that challenge most sampling-based planning methods, as it requires an accurate balance of exploration and exploitation. In AcT, the balance of exploration and exploitation depends implicitly on a single free energy functional used for policy evaluation. The results of the second study confirm the adaptivity of the exploration strategy used in AcT. They suggest that AcT can resolve challenging problems whose value functions are not smooth and are, therefore, challenging to explore systematically. The results of the third study show that AcT can successfully address POMDP problems (here, *RockSample*). The performance of AcT scales gracefully with problem size and is largely comparable with state-of-the-art POMDP algorithms, such as SARSOP (Spaan & Vlassis, 2005), AEMS2 (Shani et al., 2013), POMCP, and DESPOT (Ye et

al., 2017); see also (Silver & Veness, 2010) and (Ong et al., 2010). Even though the performance is scored by the same (average discounted reward) measure that all the planning algorithms except AcT optimise.

Finally, we used *Active Inference Tree Search* to simulate neuronal responses during a representative planning task. This simulation illustrates the ability to map the algorithmic-level planning dynamics of AcT to neuronal-level representations putatively found in the hippocampus (and other areas, such as the prefrontal cortex) of animals that solve equivalent tasks (Foster & Wilson, 2007; Pezzulo et al., 2014; Pezzulo, Kemere, et al., 2017). Indeed, active inference originated in computational and systems neuroscience, intending to characterise brain processes from a normative perspective. AcT retains the neurobiological motivation of active inference while aiming to expand it to large-scale problems that previous implementations could not address. Using AcT to both address large scale planning problems and explain neuronal activity can help establish a much-needed bridge between AI and computational neuroscience.

Declaration of conflict-of-interest

The authors have no conflict-of-interest to declare.

Acknowledgements

KJF is supported by funding for the Wellcome Centre for Human Neuroimaging (Ref: 205103/Z/16/Z) and a Canada-UK Artificial Intelligence Initiative (Ref: ES/T01279X/1), KJF and GP are supported by the European Union's Horizon 2020 Framework Programme for Research and Innovation under the Specific Grant Agreement No. 945539 (Human Brain Project SGA3). GP is supported by the European Research Council under the Grant Agreement No. 820213 (ThinkAhead). The funders had no role in study design, data collection and analysis, decision to publish, or preparation of the manuscript.

References

- Attias, H. (2003a). Planning by Probabilistic Inference. *Proceedings of the Ninth International Workshop on Artificial Intelligence and Statistics*.
- Attias, H. (2003b, January 3). Planning as Probabilistic Inference. *Proceedings of the Ninth International Workshop on Artificial Intelligence and Statistics, {AISTATS} 2003*. AISTATS 2003, Key West, Florida, USA.
- Auer, P., Cesa-Bianchi, N., & Fischer, P. (2002). Finite-time Analysis of the Multiarmed Bandit Problem. *Machine Learning*, 47(2), 235–256. <https://doi.org/10.1023/A:1013689704352>
- Badue, C., Guidolini, R., Carneiro, R. V., Azevedo, P., Cardoso, V. B., Forechi, A., Jesus, L., Berriel, R., Paixão, T., Mutz, F., Veronese, L., Oliveira-Santos, T., & De Souza, A. F. (2019). Self-Driving Cars: A Survey. *ArXiv:1901.04407 [Cs]*. <http://arxiv.org/abs/1901.04407>
- Beal, M. J. (2003). *Variational algorithms for approximate Bayesian inference*. University of London. <http://www.cse.buffalo.edu/faculty/mbeal/papers/beal03.pdf>
- Bonet, B., & Geffner, H. (2009). Solving POMDPs: RTDP-Bel versus point-based algorithms. *Twenty-First International Joint Conference on Artificial Intelligence*.
- Botvinick, M., & Toussaint, M. (2012). Planning as inference. *Trends in Cognitive Sciences*, 16(10), 485–488. <https://doi.org/10.1016/j.tics.2012.08.006>
- Botvinick, M., Wang, J. X., Dabney, W., Miller, K. J., & Kurth-Nelson, Z. (2020). Deep Reinforcement Learning and Its Neuroscientific Implications. *Neuron*, 107(4), 603–616. <https://doi.org/10.1016/j.neuron.2020.06.014>
- Brock, O., Trinkle, J., & Ramos, F. (2009). SARSOP: Efficient Point-Based POMDP Planning by Approximating Optimally Reachable Belief Spaces. In *Robotics: Science and Systems IV* (pp. 65–72). MITP. <https://ieeexplore.ieee.org/document/6284837>
- Browne, C. B., Powley, E., Whitehouse, D., Lucas, S. M., Cowling, P. I., Rohlfshagen, P., Tavener, S., Perez, D., Samothrakis, S., & Colton, S. (2012). A Survey of Monte Carlo Tree Search

- Methods. *IEEE Transactions on Computational Intelligence and AI in Games*, 4(1), 1–43.
<https://doi.org/10.1109/TCIAIG.2012.2186810>
- Cai, P., Luo, Y., Hsu, D., & Sun Lee, W. (2018, June 26). HyP-DESPOT: A Hybrid Parallel Algorithm for Online Planning under Uncertainty. *Robotics: Science and Systems XIV*. Robotics: Science and Systems 2018. <https://doi.org/10.15607/RSS.2018.XIV.004>
- Cassandra, A. R., Kaelbling, L. P., & Littman, M. L. (1994). Acting optimally in partially observable stochastic domains. *Aaai*, 94, 1023–1028.
- Champion, T., Bowman, H., & Grześ, M. (2022). Branching time active inference: Empirical study and complexity class analysis. *Neural Networks*.
- Clark, A. (2015). *Surfing Uncertainty: Prediction, Action, and the Embodied Mind*. Oxford University Press, Incorporated.
- Coquelin, P.-A., & Munos, R. (2014). Bandit Algorithms for Tree Search. *ArXiv:1408.2028 [Cs]*.
<http://arxiv.org/abs/1408.2028>
- Daw, N. D., & Dayan, P. (2014). The algorithmic anatomy of model-based evaluation. *Philosophical Transactions of the Royal Society B: Biological Sciences*, 369(1655), 20130478.
- Donnarumma, F., Maisto, D., & Pezzulo, G. (2016). Problem Solving as Probabilistic Inference with Subgoalng: Explaining Human Successes and Pitfalls in the Tower of Hanoi. *PLOS Computational Biology*, 12(4), e1004864. <https://doi.org/10.1371/journal.pcbi.1004864>
- Foster, D. J., & Wilson, M. A. (2007). Hippocampal theta sequences. *Hippocampus*, 17(11), 1093–1099. <https://doi.org/10.1002/hipo.20345>
- Fountas, Z., Sajid, N., Mediano, P. A. M., & Friston, K. (2020). Deep active inference agents using Monte-Carlo methods. *ArXiv:2006.04176 [Cs, q-Bio, Stat]*. <http://arxiv.org/abs/2006.04176>
- Friston, K., Da Costa, L., Hafner, D., Hesp, C., & Parr, T. (2020). Sophisticated Inference. *ArXiv:2006.04120 [Cs, q-Bio]*. <http://arxiv.org/abs/2006.04120>
- Friston, K., FitzGerald, T., Rigoli, F., Schwartenbeck, P., & Pezzulo, G. (2017). Active Inference: A Process Theory. *Neural Computation*, 29(1), 1–49. https://doi.org/10.1162/NECO_a_00912

- Friston, K. J. (2010). The free-energy principle: A unified brain theory *Nat Rev Neurosci*, 11(2), 127–138. <https://doi.org/10.1038/nrn2787>
- Friston, K. J., FitzGerald, T., Rigoli, F., Schwartenbeck, P., O’Doherty, J., & Pezzulo, G. (2016). Active inference and learning. *Neuroscience & Biobehavioral Reviews*, 68, 862–879. <https://doi.org/10.1016/j.neubiorev.2016.06.022>
- Friston, K. J., FitzGerald, T., Rigoli, F., Schwartenbeck, P., & Pezzulo, G. (2016). Active Inference: A Process Theory. *Neural Computation*, 1–49. https://doi.org/10.1162/NECO_a_00912
- Friston, K. J., Parr, T., & de Vries, B. (2017). The graphical brain: Belief propagation and active inference. *Network Neuroscience*, 1(4), 381–414. https://doi.org/10.1162/NETN_a_00018
- Friston, K. J., Rosch, R., Parr, T., Price, C., & Bowman, H. (2017). Deep temporal models and active inference. *Neuroscience and Biobehavioral Reviews*, 77, 388–402. <https://doi.org/10.1016/j.neubiorev.2017.04.009>
- Friston, K. J., Schwartenbeck, P., FitzGerald, T., Moutoussis, M., Behrens, T., & Dolan, R. J. (2014). The anatomy of choice: Dopamine and decision-making. *Philosophical Transactions of the Royal Society of London B: Biological Sciences*, 369(1655), 20130481. <https://doi.org/10.1098/rstb.2013.0481>
- Friston, K., Rigoli, F., Ognibene, D., Mathys, C., Fitzgerald, T., & Pezzulo, G. (2015). Active inference and epistemic value. *Cognitive Neuroscience*, 6(4), 187–214. <https://doi.org/10.1080/17588928.2015.1020053>
- Friston, K., Samothrakis, S., & Montague, R. (2012). Active inference and agency: Optimal control without cost functions. *Biological Cybernetics*, 106(8–9), 523–541.
- Friston, K., Schwartenbeck, P., FitzGerald, T., Moutoussis, M., Behrens, T., & Dolan, R. J. (2013). The anatomy of choice: Active inference and agency. *Frontiers in Human Neuroscience*, 7, 598. <https://doi.org/10.3389/fnhum.2013.00598>

- Galceran, E., Cunningham, A. G., Eustice, R. M., & Olson, E. (2017). Multipolicy decision-making for autonomous driving via changepoint-based behavior prediction: Theory and experiment. *Autonomous Robots*, 41(6), 1367–1382. <https://doi.org/10.1007/s10514-017-9619-z>
- Geffner, H. (2013). Computational models of planning. *Wiley Interdisciplinary Reviews: Cognitive Science*, 4(4), 341–356.
- Geffner, H. (2018). Model-free, Model-based, and General Intelligence. *ArXiv Preprint ArXiv:1806.02308*.
- Gelly, S., & Silver, D. (2011). Monte-Carlo tree search and rapid action value estimation in computer Go. *Artificial Intelligence*, 175(11), 1856–1875. <https://doi.org/10.1016/j.artint.2011.03.007>
- George, D., Lehrach, W., Kansky, K., Lázaro-Gredilla, M., Laan, C., Marthi, B., Lou, X., Meng, Z., Liu, Y., Wang, H., Lavin, A., & Phoenix, D. S. (2017). A generative vision model that trains with high data efficiency and breaks text-based CAPTCHAs. *Science*, 358(6368). <https://doi.org/10.1126/science.aag2612>
- Hassabis, D., Kumaran, D., Summerfield, C., & Botvinick, M. (2017). Neuroscience-Inspired Artificial Intelligence. *Neuron*, 95(2), 245–258. <https://doi.org/10.1016/j.neuron.2017.06.011>
- Huys, Q. J. M., Lally, N., Faulkner, P., Eshel, N., Seifritz, E., Gershman, S. J., Dayan, P., & Roiser, J. P. (2015). Interplay of approximate planning strategies. *Proceedings of the National Academy of Sciences of the United States of America*, 112(10), 3098–3103. <https://doi.org/10.1073/pnas.1414219112>
- Igl, M., Zintgraf, L., Le, T. A., Wood, F., & Whiteson, S. (2018). Deep Variational Reinforcement Learning for POMDPs. In J. Dy & A. Krause (Eds.), *Proceedings of the 35th International Conference on Machine Learning* (Vol. 80, pp. 2117–2126). PMLR. <http://proceedings.mlr.press/v80/igl18a.html>
- Kappen, H. J., Gómez, V., & Opper, M. (2012). Optimal control as a graphical model inference problem. *Machine Learning*, 87(2), 159–182.

- Karkus, P., Hsu, D., & Lee, W. S. (2017). QMDP-Net: Deep Learning for Planning under Partial Observability. In I. Guyon, U. V. Luxburg, S. Bengio, H. Wallach, R. Fergus, S. Vishwanathan, & R. Garnett (Eds.), *Advances in Neural Information Processing Systems 30* (pp. 4694–4704). Curran Associates, Inc. <http://papers.nips.cc/paper/7055-qmdp-net-deep-learning-for-planning-under-partial-observability.pdf>
- Kearns, M., Mansour, Y., & Ng, A. Y. (2002). A sparse sampling algorithm for near-optimal planning in large Markov decision processes. *Machine Learning*, 49(2–3), 193–208.
- Keramati, M., Smittenaar, P., Dolan, R. J., & Dayan, P. (2016). Adaptive integration of habits into depth-limited planning defines a habitual-goal-directed spectrum. *Proceedings of the National Academy of Sciences of the United States of America*, 113(45), 12868–12873. <https://doi.org/10.1073/pnas.1609094113>
- Kocsis, L., & Szepesvári, C. (2006). Bandit Based Monte-Carlo Planning. In J. Fürnkranz, T. Scheffer, & M. Spiliopoulou (Eds.), *Machine Learning: ECML 2006* (pp. 282–293). Springer. https://doi.org/10.1007/11871842_29
- Kocsis, L., Szepesvari, C., & Willemson, J. (2006). *Improved Monte-Carlo Search* (No. 1; p. 22). University of Tartu.
- Kuleshov, V., & Precup, D. (2014). Algorithms for multi-armed bandit problems. *ArXiv:1402.6028 [Cs]*. <http://arxiv.org/abs/1402.6028>
- Kurth-Nelson, Z., Economides, M., Dolan, R. J., & Dayan, P. (2016). Fast Sequences of Non-spatial State Representations in Humans. *Neuron*, 91(1), 194–204. <https://doi.org/10.1016/j.neuron.2016.05.028>
- Lee, T., & Kim, Y. J. (2016). Massively parallel motion planning algorithms under uncertainty using POMDP. *The International Journal of Robotics Research*, 35(8), 928–942. <https://doi.org/10.1177/0278364915594856>
- Levine, S. (2018). Reinforcement Learning and Control as Probabilistic Inference: Tutorial and Review. *ArXiv:1805.00909 [Cs, Stat]*. <http://arxiv.org/abs/1805.00909>

- Maisto, D., Friston, K., & Pezzulo, G. (2019). Caching mechanisms for habit formation in Active Inference. *Neurocomputing*, 359, 298–314. <https://doi.org/10.1016/j.neucom.2019.05.083>
- McAllester, D. A., & Singh, S. (n.d.). Approximate Planning for Factored POMDPs using Belief State Simplification. *Proceedings of the 15th Annual Conference on Uncertainty in Artificial Intelligence (UAI-99)*, 409–416.
- Miller, K. J., Botvinick, M. M., & Brody, C. D. (2017). Dorsal hippocampus contributes to model-based planning. *Nature Neuroscience*, 20(9), 1269–1276. <https://doi.org/10.1038/nn.4613>
- Millidge, B. (2019a). Deep Active Inference as Variational Policy Gradients. *ArXiv:1907.03876 [Cs]*. <http://arxiv.org/abs/1907.03876>
- Millidge, B. (2019b). Deep Active Inference as Variational Policy Gradients. *ArXiv:1907.03876 [Cs]*. <http://arxiv.org/abs/1907.03876>
- Mushiake, H., Saito, N., Sakamoto, K., Itoyama, Y., & Tanji, J. (2006). Activity in the lateral prefrontal cortex reflects multiple steps of future events in action plans. *Neuron*, 50(4), 631–641. <https://doi.org/10.1016/j.neuron.2006.03.045>
- Nau, D. S. (1982). An investigation of the causes of pathology in games. *Artificial Intelligence*, 19(3), 257–278. [https://doi.org/10.1016/0004-3702\(82\)90002-9](https://doi.org/10.1016/0004-3702(82)90002-9)
- Ong, S. C. W., Png, S. W., Hsu, D., & Lee, W. S. (2009). POMDPs for Robotic Tasks with Mixed Observability. *Robotics: Science and Systems*.
- Ong, S. C. W., Shao Wei Png, Hsu, D., & Wee Sun Lee. (2010). Planning under Uncertainty for Robotic Tasks with Mixed Observability. *The International Journal of Robotics Research*, 29(8), 1053–1068. <https://doi.org/10.1177/0278364910369861>
- Ortega, P. A., & Braun, D. A. (2013). Thermodynamics as a theory of decision-making with information-processing costs. *Proceedings of the Royal Society A: Mathematical, Physical and Engineering Science*, 469(2153). <https://doi.org/10.1098/rspa.2012.0683>

- Paquet, S., Tobin, L., & Chaib-Draa, B. (2005). An online POMDP algorithm for complex multiagent environments. *Proceedings of the Fourth International Joint Conference on Autonomous Agents and Multiagent Systems*, 970–977.
- Parr, T., & Friston, K. J. (2017). Uncertainty, epistemics and active inference. *Journal of The Royal Society Interface*, 14(136), 20170376. <https://doi.org/10.1098/rsif.2017.0376>
- Parr, T., & Friston, K. J. (2018). The Computational Anatomy of Visual Neglect. *Cerebral Cortex*, 28(2), 777–790. <https://doi.org/10.1093/cercor/bhx316>
- Parr, T., Pezzulo, G., & Friston, K. J. (2022). *Active Inference: The Free Energy Principle in Mind, Brain, and Behavior*. MIT Press.
- Pazis, J., & Parr, R. (2011). Non-parametric approximate linear programming for MDPs. *Proceedings of the Twenty-Fifth AAAI Conference on Artificial Intelligence*, 459–464.
- Pezzulo, G., Donnarumma, F., Iodice, P., Maisto, D., & Stoianov, I. (2017). Model-Based Approaches to Active Perception and Control. *Entropy*, 19(6), 266. <https://doi.org/10.3390/e19060266>
- Pezzulo, G., Donnarumma, F., Maisto, D., & Stoianov, I. (2019). Planning at decision time and in the background during spatial navigation. *Current Opinion in Behavioral Sciences*, 29, 69–76. <https://doi.org/10.1016/j.cobeha.2019.04.009>
- Pezzulo, G., Kemere, C., & Meer, M. van der. (2017). Internally generated hippocampal sequences as a vantage point to probe future-oriented cognition. *Annals of the New York Academy of Sciences*, 1396, 144–165.
- Pezzulo, G., Rigoli, F., & Chersi, F. (2013). The Mixed Instrumental Controller: Using Value of Information to combine habitual choice and mental simulation. *Frontiers in Cognition*, 4, 92. <https://doi.org/10.3389/fpsyg.2013.00092>
- Pezzulo, G., Rigoli, F., & Friston, K. (2018). Hierarchical Active Inference: A Theory of Motivated Control. *Trends in Cognitive Sciences*, 22(4), 294–306. <https://doi.org/10.1016/j.tics.2018.01.009>

- Pezzulo, G., Rigoli, F., & Friston, K. J. (2015). Active Inference, homeostatic regulation and adaptive behavioural control. *Progress in Neurobiology*, 136, 17–35.
- Pezzulo, G., van der Meer, M. A. A., Lansink, C. S., & Pennartz, C. M. A. (2014). Internally generated sequences in learning and executing goal-directed behavior. *Trends in Cognitive Sciences*, 18(12), 647–657. <https://doi.org/10.1016/j.tics.2014.06.011>
- Pfeiffer, B. E., & Foster, D. J. (2013). Hippocampal place-cell sequences depict future paths to remembered goals. *Nature*, 497(7447), 74–79. <https://doi.org/10.1038/nature12112>
- Pineau, J., Gordon, G., & Thrun, S. (2003). Point-based value iteration: An anytime algorithm for POMDPs. *In Proc. Int. Jnt. Conf. on Artificial Intelligence (IJCAI)*, 3, 477–484.
- Ramanujan, R., Sabharwal, A., & Selman, B. (2010). On adversarial search spaces and sampling-based planning. *Proc. 20th Int. Conf. Autom. Plan. Sched.*, 242–245.
- Rawlik, K., Toussaint, M., & Vijayakumar, S. (2013). On stochastic optimal control and reinforcement learning by approximate inference. *Twenty-Third International Joint Conference on Artificial Intelligence*.
- Redish, A. D. (2016). Vicarious trial and error. *Nature Reviews Neuroscience*, 17(3), 147–159. <https://doi.org/10.1038/nrn.2015.30>
- Ross, S., Pineau, J., & Chaib-draa, B. (2008). Theoretical Analysis of Heuristic Search Methods for Online POMDPs. *Advances in Neural Information Processing Systems*, 20, 1216–1225.
- Ross, S., Pineau, J., Paquet, S., & Chaib-draa, B. (2008). Online Planning Algorithms for POMDPs. *Journal of Artificial Intelligence Research*, 32, 663–704. <https://doi.org/10.1613/jair.2567>
- Russell, S. J., & Norvig, P. (2002). *Artificial intelligence: A modern approach (International Edition)*. <http://www.citeulike.org/group/1104/article/115157>
- Saito, N., Mushiake, H., Sakamoto, K., Itoyama, Y., & Tanji, J. (2005). Representation of immediate and final behavioral goals in the monkey prefrontal cortex during an instructed delay period. *Cereb Cortex*, 15(10), 1535–1546. <https://doi.org/10.1093/cercor/bhi032>

- Schuck, N. W., & Niv, Y. (2019). Sequential replay of nonspatial task states in the human hippocampus. *Science*, 364(6447). <https://doi.org/10.1126/science.aaw5181>
- Schwartenbeck, P., FitzGerald, T. H., Mathys, C., Dolan, R., & Friston, K. (2014). The dopaminergic midbrain encodes the expected certainty about desired outcomes. *Cerebral Cortex*, bhu159.
- Schwartenbeck, P., Passecker, J., Hauser, T. U., FitzGerald, T. H., Kronbichler, M., & Friston, K. J. (2019). Computational mechanisms of curiosity and goal-directed exploration. *ELife*, 8, e41703. <https://doi.org/10.7554/eLife.41703>
- Schwarting, W., Alonso-Mora, J., & Rus, D. (2018). Planning and Decision-Making for Autonomous Vehicles. *Annual Review of Control, Robotics, and Autonomous Systems*, 1(1), 187–210. <https://doi.org/10.1146/annurev-control-060117-105157>
- Seth, A. K. (2014). The cybernetic Bayesian brain: From interoceptive inference to sensorimotor contingencies. *MIND Project*, Eds. T. Metzinger & J. Windt.
- Shani, G., Pineau, J., & Kaplow, R. (2013). A survey of point-based POMDP solvers. *Autonomous Agents and Multi-Agent Systems*, 27(1), 1–51. <https://doi.org/10.1007/s10458-012-9200-2>
- Silver, D., & Veness, J. (2010). Monte-Carlo Planning in Large POMDPs. In J. D. Lafferty, C. K. I. Williams, J. Shawe-Taylor, R. S. Zemel, & A. Culotta (Eds.), *Advances in Neural Information Processing Systems 23* (pp. 2164–2172). Curran Associates, Inc. <http://papers.nips.cc/paper/4031-monte-carlo-planning-in-large-pomdps.pdf>
- Smith, T., & Simmons, R. (2004). Heuristic Search Value Iteration for POMDPs. *Proceedings of the 20th Conference on Uncertainty in Artificial Intelligence*, 520–527.
- Spaan, M. T. J., & Vlassis, N. (2005). Perseus: Randomized Point-based Value Iteration for POMDPs. *Journal of Artificial Intelligence Research*, 24, 195–220. <https://doi.org/10.1613/jair.1659>
- Steven, J., Konidaris, G., & Rosman, B. (2017). An analysis of monte carlo tree search. *Thirty-First AAAI Conference on Artificial Intelligence*.

- Storrs, K. R., & Kriegeskorte, N. (2019). Deep learning for cognitive neuroscience. *ArXiv Preprint ArXiv:1903.01458*.
- Sussillo, D., Churchland, M. M., Kaufman, M. T., & Shenoy, K. V. (2015). A neural network that finds a naturalistic solution for the production of muscle activity. *Nature Neuroscience*, 18(7), 1025–1033. <https://doi.org/10.1038/nn.4042>
- Sutton, R. S., & Barto, A. G. (1998). *Reinforcement Learning: An Introduction*. MIT Press.
- Teh, Y. W., Jordan, M. I., Beal, M. J., & Blei, D. M. (2006). Hierarchical dirichlet processes. *Journal of the American Statistical Association*, 101(476), 1566–1581.
- Todorov, E. (2008). General duality between optimal control and estimation. *2008 47th IEEE Conference on Decision and Control*, 4286–4292.
- Tschantz, A., Baltieri, M., Seth, A. K., & Buckley, C. L. (2019). Scaling active inference. *ArXiv:1911.10601 [Cs, Eess, Math, Stat]*. <http://arxiv.org/abs/1911.10601>
- Ueltzhöffer, K. (2017). Deep Active Inference. *ArXiv:1709.02341 [q-Bio]*. <http://arxiv.org/abs/1709.02341>
- Ueltzhöffer, K. (2018). Deep Active Inference. *Biological Cybernetics*, 112(6), 547–573. <https://doi.org/10.1007/s00422-018-0785-7>
- Wiener, N. (1948). *Cybernetics: Or Control and Communication in the Animal and the Machine*. The MIT Press.
- Yamins, D. L. K., & DiCarlo, J. J. (2016). Using goal-driven deep learning models to understand sensory cortex. *Nature Neuroscience*, 19(3), 356–365. <https://doi.org/10.1038/nn.4244>
- Ye, N., Somani, A., Hsu, D., & Lee, W. S. (2017). DESPOT: Online POMDP Planning with Regularization. *Journal of Artificial Intelligence Research*, 58, 231–266. <https://doi.org/10.1613/jair.5328>
- Yoon, S., Fern, A., Givan, R., & Kambhampati, S. (2008). Probabilistic planning via determinization in hindsight. *Proceedings of the National Conference on Artificial Intelligence*, 2, 1010–1016.

Appendix

A.1: Active Inference Tree Search algorithm with subroutines

```

function AcT(A, B, C, D,  $\delta$ )
     $t \leftarrow 0$ 
    while halting conditions are not satisfied do
         $\mathbf{x}_t \leftarrow$  update expected state belief  $\mathbf{x}_{t-1}$  by using  $s_t, o_t, a_{t-1}, \mathbf{A}, \mathbf{B}, \mathbf{D}$ 
        create a node  $v(\mathbf{x}_t, u_{t-1})$ 
        while  $\delta^\tau < \varepsilon$  do
             $v_\tau \leftarrow$  TreePolicy( $v, \mathbf{B}$ )
             $G_\Delta \leftarrow$  Eval( $v_\tau, \mathbf{A}, \mathbf{B}, \mathbf{C}, \delta$ )
            PathIntegration( $v_\tau, G_\Delta$ )
        End
         $(s_{t+1}, o_{t+1}, \mathbf{x}_t, a_t) \leftarrow$  extract information saved in  $v$ 
         $t \leftarrow t + 1$ 
    end
end

```

```

function TreePolicy( $v$ )
    while  $v$  is nonterminal do
        if  $v$  not fully expanded then
            return Expansion( $v, \mathbf{B}$ )
        else
             $v \leftarrow$  VariationalInference( $v$ )
        end
    end
    return  $v_\tau \leftarrow v$ 
end

```

```

function Expansion( $v, \mathbf{B}$ )
    draw randomly an unused action  $u'$  on  $v$ 
    for the parent  $v$ , generate a new child  $v'(\mathbf{x}', u')$  with  $\mathbf{x}' = \mathbf{B}(u') \cdot \mathbf{x}$ 
    return  $v'$ 
end

```

```

function VariationalInference( $v$ )
    build the distribution  $\mathbf{E}$  via the probability mass function  $\sqrt{\frac{2 \ln N(v)}{N(v)}}$ 
     $u' \sim \sigma(\kappa_p \ln \mathbf{E} - \gamma \cdot G_\Delta(v'))$ 
    return  $v'(u')$ 
end

```

```

function Eval( $v_\tau$ , A, B, C,  $\delta$ )
    evaluate the expected free energy  $G(*, v_\tau)$  through A, B, C
    return  $G_\Delta = \delta^\tau \cdot G(*, v_\tau)$ 
end

function PathIntegration( $v_\tau$ ,  $G_\Delta$ )
    while  $v_\tau$  is not  $v$  do
         $N(v_\tau) \leftarrow N(v_\tau) + 1$ 
         $G(v_\tau) \leftarrow G(v_\tau) + \frac{1}{N(v_\tau)} (G_\Delta - G(v_\tau))$ 
         $v_\tau \leftarrow \text{parent of } v_\tau$ 
    end
end

```

A.2 An example generative model: the case of *RockSample(2,1)*.

Here, we provide an example of how a POMDP problem can be represented in Active Inference. We focus on the *RockSample*(n, k) problem with $n = 2$ and $k = 1$. In this scenario, the rover explores an alien soil grid of side 2, with a unique rock to analyse, see Figure A.1. The rover starts its exploration from the top-left corner and has to reach the exit on the right side after (optionally) collecting a sample of the rock. The position of the rock in the maze and its quality ("good" or "bad") are selected randomly. In our example, the rock is placed in the bottom-right corner of the maze, and its quality is "good". Figure A.1 shows the initial configuration of the problem: the locations of the rover are denoted with " R_i " (with R_1 being the initial location), the location of the rock is denoted with " ϵ ", the exit state is denoted with "EXIT", and the grid border (that the rover cannot cross) is denoted with the symbol "*".

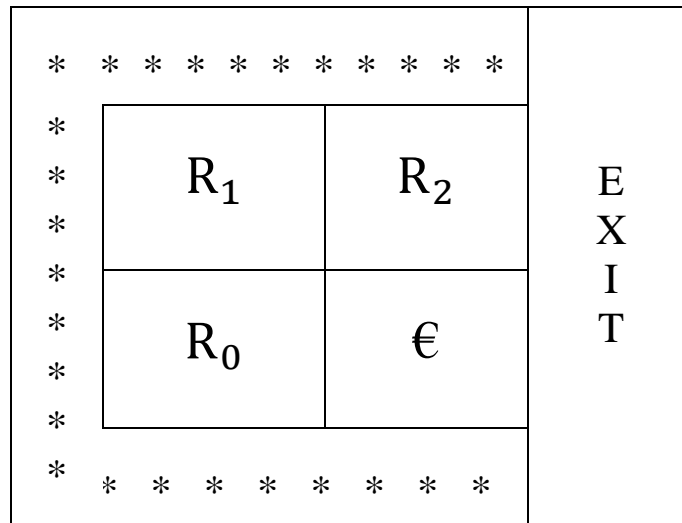


Figure A.1. The configuration of the *RockSample*(2,1) problem that we consider in our example. See the main text for illustration of the symbols.

The generative model used by the Active Inference agent is defined by setting the hidden states S , the observations O , the control states U , and the parameters $\Theta = \{\mathbf{A}, \mathbf{B}, \mathbf{C}, \mathbf{D}\}$.

As discussed in Section 4.3 of the main text, we decided not to factorize the hidden states S . Hence, with $n = 2$ and $k = 1$, the cardinality of S is $(n^2 + 1) \cdot 2^k + 1 = 11$. See Fig. A.2. Note that each location corresponds to two states (e.g., the top-left location corresponds to states 4 and 5): one in which the only rock of the problem is bad (state 4) and the other in which the rock is good (state 5). The states 8, 9, and 10 are absorbing states; the former two states correspond to the EXIT location when the rock is bad (state 8) and when it is good (state 9), and the latter state corresponds to the border. The agent's initial belief is the vector $\mathbf{D} = [0, 0, 0.5, 0.5, 0, 0, 0, 0, 0, 0]^T$, which implies that it knows it starts from the top-left location, but it does not know whether the rock is bad or good (hence it considers equally probably starting from state 4 or 5).

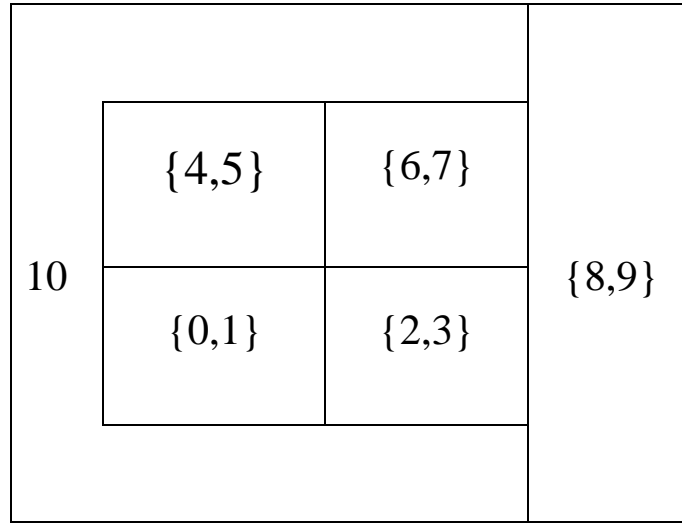


Fig. A.2 Mapping between the 11 hidden states and the 6 grid locations of the *RockSample(2,1)* problem. See the main text for explanation.

Observations O are organized in three factors, that is:

$$O \equiv [o_{R_0}, o_{\epsilon}, o_{R_1}, o_{R_2}, o_{\text{EXIT}}, o_*]^T \otimes [\text{bad}, \text{good}]^T \otimes [\text{reward}, \text{penalty}]^T.$$

The first factor describes the 6 locations of the maze and therefore has size 6. The second factor describes all the possible 2^k possible combinations of rock qualities, good or bad (for $k = 1$, this factor has size 2). The third factor describes the utility (reward or penalty) of the current state. By considering that the main goal of the rover is obtaining rewards, the prior over (preferred) observations is:

$$\mathbf{C} = [1/6, 1/6, 1/6, 1/6, 1/6, 1/6]^T \otimes [0.5, 0.5]^T \otimes [c, -c]^T, \text{ with } c > 0.$$

The control states U encode the actions of the agent. These are: go north (gn), go south (gs), go west (gw), go east (ge), check the rock from remote (cr) with variable accuracy, and collect a sample of the rock (sr). Note that for $k > 1$, there are k additional remote sensing actions, one for each rock.

Note also that the action cr changes the quality of the sampled rock from "good" to "bad", or leaves it unaltered if the rock was already bad.

The control states U determine the transitions from one state to another, as specified by the set of matrices \mathbf{B}_u shown below, one for each control state u .

$$\mathbf{B}_{gn} = \begin{pmatrix} 0 & & & & & & & & & & \\ \vdots & & & & & & & & & & \\ & 0 & \vdots & & & & & & & & \\ & 1 & 0 & \vdots & & & & & & & \\ & 0 & 1 & 0 & \vdots & & & & & & \\ & \vdots & 0 & 1 & 0 & & & & \vdots & & \\ & & \vdots & 0 & 1 & & & & 0 & \vdots & \\ & & & \vdots & 0 & \vdots & \vdots & \vdots & 1 & 0 & \vdots \\ & & & & 0 & 0 & 0 & 0 & 0 & 1 & 0 \\ & & & & 0 & 1 & 1 & 1 & 1 & 0 & 1 \end{pmatrix}$$

$$\mathbf{B}_{gs} = \begin{pmatrix} 0 & \dots & & 0 & 1 & 0 & \dots & & & & \\ \vdots & & & & 0 & 1 & 0 & \dots & & & \\ & & & & \vdots & 0 & 1 & 0 & & & \\ & & & & & \vdots & 0 & 1 & & & \\ & & & & & & \vdots & 0 & & & \\ & & & & & & & \vdots & & & \\ & & & & & & & & \vdots & & \\ & & & & & & & & 0 & \vdots & \\ & \vdots & \vdots & \vdots & \vdots & & & & 1 & 0 & \vdots \\ & 0 & 0 & 0 & 0 & \dots & & & 0 & 1 & 0 \\ & 1 & 1 & 1 & 1 & 0 & \dots & & \dots & 0 & 1 \end{pmatrix}$$

$$\mathbf{B}_{gw} = \begin{pmatrix} 0 & 0 & 1 & 0 & \dots & & & & & & \\ \vdots & \vdots & 0 & 1 & & & & & & & \\ & & \vdots & 0 & & & \vdots & & & & \\ & & & \vdots & & & 0 & \vdots & & & \\ & & & & & & 1 & 0 & & & \\ & & & & & & 0 & 1 & & & \\ & & & & & & \vdots & 0 & \vdots & & \\ & & & & & & & \vdots & 0 & \vdots & \\ & \vdots & \vdots & & \vdots & \vdots & & & 1 & 0 & \vdots \\ & 0 & 0 & & 0 & 0 & \vdots & \vdots & 0 & 1 & 0 \\ & 1 & 1 & & 1 & 1 & 0 & 0 & 0 & 0 & 1 \end{pmatrix}$$

$$\begin{aligned}
\mathbf{B}_{ge} &= \begin{pmatrix} 0 & & & & & & & & & & \\ 0 & \vdots & & & & & & & & & \\ 1 & 0 & & & & & & & & & \\ 0 & 1 & & & & & & & & & \\ \vdots & 0 & & & \vdots & & & & & & \\ & \vdots & & & 0 & \vdots & & & & & \\ & & & & 1 & 0 & \vdots & & \vdots & & \\ & & 0 & \vdots & 0 & 1 & 0 & \vdots & 0 & \vdots & \\ & & 1 & 0 & \vdots & 0 & 1 & 0 & 1 & 0 & \vdots \\ & & 0 & 1 & & \vdots & 0 & 1 & 0 & 1 & 0 \\ & & 0 & 0 & & & 0 & 0 & 0 & 0 & 1 \end{pmatrix} \\
\mathbf{B}_{cr} &= \begin{pmatrix} 1 & 0 & \dots & & & & & & & & \\ 0 & \ddots & & & & & & & & & \\ \vdots & & & & & & & & & & \\ & & & \ddots & & & & & & & \\ & & & & 1 & & & & & & \\ & & & & & \ddots & & & & & \\ & & & & & & & & & \vdots & \\ & & & & & & & & \ddots & 0 & \\ & & & & & & & \dots & 0 & 1 \end{pmatrix} \\
\mathbf{B}_{sr} &= \begin{pmatrix} 1 & 0 & 0 & 0 & & & & & & & \\ 0 & 1 & 0 & 0 & & & & & & & \\ \vdots & 0 & 1 & 1 & \vdots & & & & & & \\ & \vdots & 0 & 0 & 0 & \vdots & & & & & \\ & & \vdots & \vdots & 1 & 0 & \vdots & & & & \\ & & & & 0 & 1 & 0 & \vdots & & & \\ & & & & \vdots & 0 & 1 & 0 & \vdots & & \\ & & & & & \vdots & 0 & 1 & 0 & \vdots & \\ & & & & & & \vdots & 0 & 1 & 0 & \vdots \\ & & & & & & & 0 & 1 & 0 & \\ & & & & & & & 0 & 0 & 1 \end{pmatrix}
\end{aligned}$$

Furthermore, the control states U determine the likelihood mapping from hidden states to observations, as specified in the matrix \mathbf{A} . Note that the matrix \mathbf{A} has three components, one for each factor of the observations. The first component A_u^1 , which describes the 6 locations of the maze, is the same for each u :

$$A_u^1 = \begin{pmatrix} 1 & 1 & 0 & 0 & 0 & 0 & & & & & \\ 0 & 0 & 1 & 1 & 0 & 0 & \vdots & \vdots & & & \\ \vdots & \vdots & 0 & 0 & 1 & 1 & 0 & 0 & \vdots & \vdots & \\ & & \vdots & \vdots & 0 & 0 & 1 & 1 & 0 & 0 & \vdots \\ & & & \vdots & \vdots & 0 & 0 & 1 & 1 & 0 & \\ & & & & & 0 & 0 & 0 & 0 & 1 \end{pmatrix}, \forall u \in U$$

The second component A_u^2 , which describes the observed rock configuration, is different depending on the control state u set. For u expressing movements, namely $u \in \{gn, gs, gw, ge\}$, A_u^2 is:

$$A_{\{gn,gs,gw,ge\}}^2 = \begin{pmatrix} 1 & 0 & 1 & 0 & 1 & 0 & 1 & 0 & 1 & 0 & 0.5 \\ 0 & 1 & 0 & 1 & 0 & 1 & 0 & 1 & 0 & 1 & 0.5 \end{pmatrix}.$$

For $u = cr$, the A_{cr}^2 elements are computed by considering that the probability of observing the rock quality depends only on the rover position R and is independent of the other rock qualities. The probability that the sensor is accurate on the rock is $P_{ac|R_i,cr} \equiv P(\text{accurate} | R_i, cr) = (1 + \eta(R_i, \epsilon)) / 2$; where $\eta(R_i, \epsilon) = 2^{-d(R_i, \epsilon)/d_0}$, with $d(R_i, \epsilon)$ denoting the Euclidean distance between the positions R_i and ϵ , and d_0 is a constant specifying the half accuracy distance. In our case, there is only one rock, and its quality is “good”. Therefore, A_{cr}^2 is:

$$A_{cr}^2 = \begin{pmatrix} \bar{P}_{ac|R_0,cr} & \bar{P}_{ac|R_0,cr} & 0 & 0 & \bar{P}_{ac|R_1,cr} & \bar{P}_{ac|R_1,cr} & \bar{P}_{ac|R_2,cr} & \bar{P}_{ac|R_2,cr} & 1 & 0 & 0.5 \\ P_{ac|R_0,cr} & P_{ac|R_0,cr} & 1 & 1 & P_{ac|R_1,cr} & P_{ac|R_1,cr} & P_{ac|R_2,cr} & P_{ac|R_2,cr} & 0 & 1 & 0.5 \end{pmatrix}$$

where $\bar{P}_{ac|R_i,cr} = 1 - P_{ac|R_i,cr}$.

The third component A_u^3 , which describes the utility value associated with the observed outcome, is different depending on the control state u set. The A_{sr}^3 matrix for the control state $u = sr$ is the following:

$$A_{sr}^3 = \begin{pmatrix} 0 & 0 & 0 & 1 & 0 & 0 & 0 & 0 & 0.5 & 0.5 & 0.5 \\ 1 & 1 & 1 & 0 & 1 & 1 & 1 & 1 & 0.5 & 0.5 & 0.5 \end{pmatrix}$$

The A_{sr}^3 matrix for all the other control states $u \in \{gn, gs, gw, ge, cr\}$ is the following:

$$A_{\{gn,gs,gw,ge,cr\}}^3 = \begin{pmatrix} 0.5 & \dots & \dots & 0.5 & 1 & 0 & 0 \\ 0.5 & \dots & \dots & 0.5 & 0 & 1 & 1 \end{pmatrix}$$

where the first and second rows encode the probability of observing a reward and a penalty, respectively.

The overall A_u^3 matrix reflects the fact that the only two ways to observe a reward are collecting a sample of the good rock (i.e., being in state 3) and going to the EXIT after having collected a sample of the good rock (i.e., being in state 8, which implies that the rock is bad - which is possible after a sample of the good rock has been collected and the good rock has been changed in a bad rock). Rather, the agent gets a penalty if it reaches the EXIT without having collected a sample of the good rock, or if it reaches the border at any time.